

This is a repository copy of *Modeling lightning-NOx chemistry on a sub-grid scale in a global chemical transport model*.

White Rose Research Online URL for this paper:

<https://eprints.whiterose.ac.uk/100006/>

Version: Published Version

Article:

Gressent, A., Sauvage, B., Cariolle, D. et al. (4 more authors) (2016) Modeling lightning-NOx chemistry on a sub-grid scale in a global chemical transport model. Atmospheric Chemistry and Physics. pp. 5867-5889. ISSN 1680-7324

<https://doi.org/10.5194/acp-16-5867-2016>

Reuse

This article is distributed under the terms of the Creative Commons Attribution (CC BY) licence. This licence allows you to distribute, remix, tweak, and build upon the work, even commercially, as long as you credit the authors for the original work. More information and the full terms of the licence here:

<https://creativecommons.org/licenses/>

Takedown

If you consider content in White Rose Research Online to be in breach of UK law, please notify us by emailing eprints@whiterose.ac.uk including the URL of the record and the reason for the withdrawal request.



Modeling lightning-NO_x chemistry on a sub-grid scale in a global chemical transport model

Alicia Gressent¹, Bastien Sauvage¹, Daniel Cariolle^{2,3}, Mathew Evans⁴, Maud Leriche¹, Céline Mari¹, and Valérie Thouret¹

¹LA, CNRS, Université de Toulouse, Toulouse, France

²Météo France, Toulouse, France

³Centre Européen de Recherche et de Formation Avancée en Calcul Scientifique, CERFACS, Toulouse, France

⁴The Wolfson Atmospheric Chemistry Laboratories, University of York, York, UK

Correspondence to: Alicia Gressent (alicia.gressent@aero.obs-mip.fr)

Received: 20 October 2015 – Published in Atmos. Chem. Phys. Discuss.: 4 December 2015

Revised: 29 February 2016 – Accepted: 2 May 2016 – Published: 13 May 2016

Abstract. For the first time, a plume-in-grid approach is implemented in a chemical transport model (CTM) to parameterize the effects of the nonlinear reactions occurring within high concentrated NO_x plumes from lightning NO_x emissions (LNO_x) in the upper troposphere. It is characterized by a set of parameters including the plume lifetime, the effective reaction rate constant related to NO_x–O₃ chemical interactions, and the fractions of NO_x conversion into HNO₃ within the plume. Parameter estimates were made using the Dynamical Simple Model of Atmospheric Chemical Complexity (DSMACC) box model, simple plume dispersion simulations, and the 3-D Meso-NH (non-hydrostatic mesoscale atmospheric model). In order to assess the impact of the LNO_x plume approach on the NO_x and O₃ distributions on a large scale, simulations for the year 2006 were performed using the GEOS-Chem global model with a horizontal resolution of 2° × 2.5°. The implementation of the LNO_x parameterization implies an NO_x and O₃ decrease on a large scale over the region characterized by a strong lightning activity (up to 25 and 8 %, respectively, over central Africa in July) and a relative increase downwind of LNO_x emissions (up to 18 and 2 % for NO_x and O₃, respectively, in July). The calculated variability in NO_x and O₃ mixing ratios around the mean value according to the known uncertainties in the parameter estimates is at a maximum over continental tropical regions with ΔNO_x [–33.1, +29.7] ppt and ΔO₃ [–1.56, +2.16] ppb, in January, and ΔNO_x [–14.3, +21] ppt and ΔO₃ [–1.18, +1.93] ppb, in July, mainly depending on the determination of the diffusion properties of the atmosphere

and the initial NO mixing ratio injected by lightning. This approach allows us (i) to reproduce a more realistic lightning NO_x chemistry leading to better NO_x and O₃ distributions on the large scale and (ii) to focus on other improvements to reduce remaining uncertainties from processes related to NO_x chemistry in CTM.

1 Introduction

Lightning emissions are one of the most important sources of nitrogen oxides (NO_x ≡ NO + NO₂) in the upper troposphere (WMO, 1999; Hudman et al., 2007). Lightning primarily produces NO and may also induce a negligible quantity of NO₂ with a ratio NO₂/NO_x of 0.5 to 0.1 (Franzblau, 1991; Stark et al., 1996). NO_x emitted by lightning (LNO_x) impacts the tropospheric ozone burden (Stockwell et al., 1999; Hauglustaine et al., 2001; Grewe, 2007) and the hydroxyl-radical (OH) concentrations influencing the oxidizing capacity of the atmosphere (Labrador et al., 2004; Banerjee et al., 2014). Most NO_x produced by lightning is detrained into the free and upper troposphere, where ozone production efficiencies (OPEs) per unit NO_x emitted are 4 to 20 times higher than at the surface (Sauvage et al., 2007a; Martin et al., 2007), and therefore lightning exerts a disproportionately stronger effect on photochemistry than surface emissions (Pickering et al., 1990; Hauglustaine et al., 1994; Zhang et al., 2003; Choi et al., 2009). The longer NO_x lifetime in the upper troposphere (1–2 weeks) allows

the long-range transport of LNO_x through large circulation patterns (Hemispheric Transport of Air Pollution, HTAP, report, 2010: <http://www.htap.org/>).

Although the importance of the LNO_x emissions for the upper tropospheric chemistry is well known, it remains highly uncertain, with a best estimate of 2–8 TgN × yr⁻¹ (Schumann and Huntrieser, 2007). Lightning NO_x emissions are associated with deep convection (horizontal scale ~ 10 km) and correspond to the “sub-grid” in global chemical transport models (horizontal resolution ~ 100 s km). Therefore, lightning NO_x production must be parameterized for inclusion into a large-scale model. Global models commonly use convection proxies such as the cloud top height (Price and Rind, 1992) and the updraft intensity to estimate the lightning flashes. Flashes simulated by chemical transport models (CTMs) are commonly constrained by satellite observations (Sauvage et al., 2007b; Murray et al., 2012) from the spaceborne Lightning Imaging Sensor (LIS) in the Tropical Rainfall Measuring Mission (TRMM) and the Optical Transient Detector (OTD) (Christian et al., 2003; Tost et al., 2007). The lightning NO_x emissions are then redistributed according to a vertical profile – generally a reverse “C-Shape” profile (Ott et al., 2010) – a priori defined depending on season, latitude, and continent/ocean location. Also, corrections to the calculations of lightning NO_x emissions using satellite observations (SCIAMACHY, SCanning Imaging Absorption SpectroMeter for Atmospheric CHarotographY; Martin et al., 2007) and in situ measurements (INTEX-NA, Intercontinental Chemical Transport Experiment – North America; Hudman et al., 2007) are usually applied.

Despite the necessity of including lightning NO_x emissions in global models, the small-scale nature of the flashes and the nonlinear chemistry (Lin et al., 1988) of the atmosphere will lead to biases on the large scale with instantaneous dilution of gases in the large grid box volume. It seems likely that this will lead to an overestimate of the OPE and an underestimate of the nitric acid (HNO₃) production. For instance, by forcing NO_x concentration in a GEOS-Chem grid box over southeast Asia to represent the measured lightning plumes, Cooper et al. (2014) estimated a ratio for O₃ to HNO₃ produced leading to a 15 mol mol⁻¹ OPE in lightning plumes, which reinforces the fact that instantaneous dilution in global model implies issues in sub-grid chemistry.

In this work, a more realistic lightning NO_x chemistry as well as a plume parameterization is implemented into a global CTM allowing us to reproduce the NO_x and O₃ distributions more accurately on a large scale. The plume approach used in this study was previously developed by Carolle et al. (2009) for aircraft NO_x emissions in the LMDz-INCA (Laboratoire de Météorologie Dynamique, INteraction avec la Chimie et les Aérosols) and MOBIDIC (MOBile DIgital Compute) models and also implemented to deal with ship NO_x emissions (Huszar et al., 2010). This approach avoids the double count in the CTM calculation of

the emitted NO_x, which is first instantaneously diluted onto the point grid and secondly as the plume form. In addition, the plume parameterization is the first that considers the NO_x from lightning as a plume, with the transport of the related nonlinear chemistry effects. NO_x from lightning emissions are emitted in the upper troposphere, characterized by strong winds allowing the large-scale transport of trace species. Thus, it is relevant to consider plume growth from lightning emissions, which may have been diluted a long time after the initial lightning pulse, downwind of emissions. Consequently, the plume parameterization previously developed for aircraft exhausts has been adjusted to LNO_x emissions and implemented into the GEOS-Chem global chemical transport model.

Section 2 gives a description of the GEOS-Chem model in which the plume-in-grid parameterization is implemented and the models which are used to evaluate the diffusion properties of the atmosphere and to determine parameters characterizing the physics and chemistry of the lightning NO_x plume. A concise description of the plume approach is then presented in Sect. 3, followed by a detailed explanation of the determination of parameters related to LNO_x emissions. Section 4 summarizes the results of the simulations performed with GEOS-Chem and finally these results and the sensitivity to NO_x and O₃ variations of the parameterization are discussed in Sect. 5.

2 Models

Three different models are used in this evaluation and are described in this section. GEOS-Chem is used to provide a global framework to assess the impact of lightning NO_x. Meso-NH (non-hydrostatic mesoscale atmospheric model) is used to provide estimates of the plume diffusion timescales, and Dynamical Simple Model of Atmospheric Chemical Complexity (DSMACC) is a box model used to assess the nonlinear chemistry in the plume.

2.1 The GEOS-Chem chemical transport model

The GEOS-Chem chemical transport model (Bey et al., 2001) is a global 3-D model of atmospheric composition driven by an assimilated meteorology from the Goddard Earth Observing System (GEOS-5) of the NASA Global Modeling Assimilation Office (GMAO). The 09-01-01 version (http://wiki.seas.harvard.edu/geos-chem/index.php/GEOS-Chem_v9-01-01) of the CTM has been used in this study. The model transports 43 tracers to describe tropospheric O₃–NO_x–VOC (volatile organic compound) chemistry. The horizontal resolution is 2° × 2.5°, and 47 vertical levels are defined from the ground to 80 km altitude. The CTM includes modules for emissions, transport, chemistry, deposition, aerosols, and surface.

The large-scale advection of tracers is performed using the TPCORE advection scheme (Lin and Rood, 1996), corresponding to a semi-Lagrangian flux method. Shallow and deep moist convection processes are carried out using the relaxed Arakawa–Schubert scheme (Moorthi and Suarez, 1991). Mixing in the lower atmospheric layers is represented by a nonlocal scheme of the planetary boundary layer described by Lin and McElroy (2010). The wet deposition for water-soluble aerosols and for gases follows Liu et al. (2001) and Amos et al. (2012). Aerosol scavenging by ice crystals and cold or mixed precipitation is also reproduced in the model (Wang et al., 2011). The dry deposition is associated with a scheme which calculates bulk surface resistance in series (Wesely, 1989). Photolysis rates are calculated with the Fast-JX code (Bian and Prather, 2002). The atmospheric chemistry is resolved using the SMVGEAR (sparse-matrix vectorized gear code) solver (Jacobson and Turco, 1994), with more than 300 species and 785 chemical reactions. Heterogeneous chemical reactions are represented on the surface of aerosols (Bey et al., 2001; Martin et al., 2002). The effects of aerosols on the photolysis rates are based on Martin et al. (2003). Primary NO_x and VOC emissions are separated depending on sources. Global anthropogenic emissions are given by the GEIA (Global Emissions Initiative; Wang et al., 1998) and EGDAR (Emission Database for Global Atmospheric Research; Olivier, 2005) inventories, and regional anthropogenic emissions exceed those for the US (National Emissions Inventory, NEI05), Canada (Criteria Air Contaminants, CAC), Mexico (Big Bend Regional Aerosol and Visibility Observational study, BRAVO), Europe (EMEP, European Monitoring and Evaluation Programme), and east Asia (Streets et al., 2006; Zhang et al., 2009). Biofuel emissions are provided by the EPA (Environmental Protection Agency) and STREETS 2006 inventories (Yevich and Logan, 2003), biomass burning emissions by the GFED (Global Fire Emissions Database) inventory (van der Werf et al., 2010), and biogenic emissions by the MEGAN (Model of Emissions of Gases and Aerosols from Nature) model calculations (Guenther et al., 2012). In addition, NO_x from soil emissions is calculated by an algorithm depending on temperature and precipitation (Yienger and Levy, 1995).

In order to calculate the NO_x from lightning, flash rates are first calculated in active deep convection using the Price and Rind scheme based on cloud top height (Price and Rind, 1992, 1994); then flash rates are adjusted with local scaling factors to match the satellite climatology (Sauvage et al., 2007b; Murray et al., 2012), and the total column emissions are determined using NO_x yields that differ in the tropics and northern extratropics. Finally, the total column is distributed vertically using the reverse C-shaped profile from Ott et al. (2010). Note that the base lightning NO_x scheme is described in detail by Murray et al. (2012).

2.2 The Meso-NH model

The Meso-NH model is an atmospheric model developed jointly by the Laboratoire d'Aérologie and by CNRM-GAME (<http://mesonh.aero.obs-mip.fr/mesonh51>). The model includes a non-hydrostatic and anelastic system of equations (Lafore et al., 1998) and has a complete set of parameterizations allowing us to reproduce physical processes such as radiation (Gregory et al., 2000), atmospheric turbulence (Cuxart et al., 1999), convection (Bechtold et al., 2000), microphysics related to warm clouds (Cohard and Pinty, 2000), and atmospheric ice (Pinty and Jabouille, 1999; Lascaux et al., 2006). Meso-NH includes also online chemistry (Tulet et al., 2003, 2006). The model deals with large (synoptic) to small (large eddy) scales. In this study, the Mesonh-49 version was used in order to compare the horizontal diffusion coefficient (D_h) estimate within the anvil of thunderstorms from in situ measurements to a modeling ideal case of a convective cell.

2.3 The DSMACC box model

The DSMACC is a simple box model developed for improving our understanding of the tropospheric chemistry (Emmerson and Evans, 2009). The model is composed of the KPP (kinetic preprocessor) chemical preprocessor (Damian et al., 2002) to solve differential equations representing the chemical system. The TUV (Tropospheric Ultraviolet and Visible Radiation Model) photolysis scheme is used, which calculates the spectral irradiance, the spectral actinic flux, photodissociation coefficients (J values) (Madronich and Flocke, 1999), and biologically effective irradiance. The chemical scheme used derives from the Master Chemical Mechanism (MCM, <http://mcm.leeds.ac.uk/MCM/>), (Jenkin et al., 1997; Saunders et al., 2003), which contains 17 000 elementary reactions of 6700 primary, secondary, and radical species.

In order to study the chemical interactions that can occur in the undiluted plume fraction, a set of short simulations was carried out with the DSMACC box model as explained in Sect. 3.2.2.

2.4 The simple plume dispersion model

To model the dispersion of lightning NO_x emissions we use a simple dispersion model similar to the plume model used for aircraft NO_x emissions, except that the plume is supposed to be oriented along a vertical axis. The plume is represented as a cylinder that encompasses horizontal diffusion with a constant coefficient D_h (Sect. 3.2.1). This simple model is composed of 30 horizontal circles with spacing increasing progressively from the center axis. The discretization of the diffusion equation is mass conservative.

The chemistry scheme and associated reaction rate constants are adapted from the large-scale chemical model

MOCAGE (Modèle de Chimie Atmosphérique de Grande Echelle; Teysseire et al., 2007). It includes the main reactions involved in the NO_x–HO_x system. Simple plume simulations were performed in order to estimate the physical and chemical characteristics of the plumes related to lightning NO_x emissions.

3 Plume parameterization for lightning NO_x emissions

3.1 General description

The LNO_x plume parameterization is based on a method initially developed by Cariolle et al. (2009) for NO_x emissions related to aircraft exhausts later adapted to ship emissions of NO_x (Huszar et al., 2010). In this approach, the plume effects on a sub-grid scale are represented via a fuel tracer in order to follow the amount of the emitted species in the plume and an effective reaction rate for the ozone production and nitric acid production and destruction during the plume's dilution in the background (Cariolle et al., 2009; Paoli et al., 2011). The parameterization requires a proper estimation of the characteristic plume lifetime, during which the nonlinear interactions between species are important and simulated via specific rates of conversion. The approach ensures the mass conservation of species in the model. This is the only method which considers a plume evolution related to the local NO_x emissions, allowing the transport of the nonlinear effects which occur on a smaller scale than the model grid.

3.1.1 Physical plume formulation

Following Cariolle et al. (2009), a passive tracer (from the perspective of the usual model chemistry) is added to the CTM to represent NO_x emitted by lightning. The LNO_x tracer initial mass corresponds to the NO_x mass at the start time of the simulation. Rather than increasing the concentration of NO_x within the CTM, lightning NO_x emissions now increase the concentration of this new passive tracer, which is transported in the standard way by advection and turbulence. Plume chemistry is considered to be significant when the mixing ratio of the lightning NO_x tracer is higher than the critical NO_x content, hereafter denoted r_1 . Above this value the lightning NO_x tracer is transferred to the normal NO_x tracer at a rate described by a plume lifetime (τ), which is an exponential decay constant. This corresponds to an exchange timescale between the lightning NO_x plume and the background NO_x. The continuity equation related to the tracer evolution is detailed by Eq. (1).

$$\frac{\partial \overline{r_{\text{LNO}_x}}}{\partial t} + \langle F_{\text{LNO}_x} \rangle = I - \frac{1}{\tau} \cdot \overline{r_{\text{LNO}_x}}, \quad (1)$$

where $\overline{r_{\text{LNO}_x}}$ is the mixing ratio (in ppb) of the NO_x lightning tracer in the model grid (note that all overlined terms refer to grid average quantities in the CTM), $F_{\text{LNO}_x} \equiv \nabla \times$

$(\overline{r_{\text{LNO}_x}} u) + \nabla \times (D_t \nabla \overline{r_{\text{LNO}_x}})$ and corresponds to the flux divergence related to the large-scale transport of the tracer (advection and turbulent diffusion, in molecules cm⁻² s⁻¹), I is the injection rate of LNO_x (in s⁻¹), and τ is the plume lifetime (in seconds).

The calculation of τ requires evaluating the mass fraction of the lightning NO_x ($M(t)$) corresponding to the undiluted fraction of the plume and characterized by an NO_x mixing ratio above the r_1 critical value. In other words, the plume boundary is defined by the critical value r_1 depending on the time of day. The NO_x mass, $M(t)$, decreases monotonically to zero until $t = T_1$ for which the tracer mixing ratio is everywhere below the r_1 threshold. The plume lifetime is obtained by an exponential function depending on the mass (Eqs. 2 and 3):

$$M(t) = \int_{V_p} \rho \cdot r_p \cdot dV, \quad (2)$$

$$\tau = \int_{t_0=0}^{+\infty} \exp(-t/\tau) \cdot dt = \frac{1}{M(t_0)} \int_{t_0=0}^{T_1} M(t) \cdot dt. \quad (3)$$

Where V_p is the volume of the plume, ρ is the density of the air, r_p is the NO_x mixing ratio within the plume (in ppb), and T_1 is the time for which the mixing ratio r_p is below the critical value r_1 everywhere. The calculation of the plume lifetime, by simple plume dispersion simulations, depends on (i) the initial emissions of NO_x by lightning, (ii) the r_1 value, and (iii) the dispersion properties of the atmosphere (related to the horizontal diffusion coefficient, D_h) and is detailed in Sect. 3.2.3. Note that the mean dispersion properties of the atmosphere were associated with the horizontal diffusion only. The lightning NO_x emissions occur in the convective part of clouds where the vertical diffusion is strong. Therefore, the vertical diffusion coefficient is a determining parameter for the LNO_x distribution in the cloud. As mentioned in Sect. 2.1, the vertical distribution of LNO_x is calculated a priori from Ott et al. (2010) as a reverse C-shaped profile. The LNO_x plume parameterization is applied a posteriori; after that, lightning NO_x is vertically prescribed and concerns convective outflow where NO_x is detrained in the troposphere. In this region of detrainment, the horizontal dispersion may be more efficient than the vertical one as discussed in Cariolle et al. (2009).

3.1.2 Plume chemistry of NO_x, O₃, and HNO₃

Once the lightning NO_x is emitted, it is transferred to model's background NO_x based on the lifetime of the plume (τ). Thus, the continuity equation for the NO_x species emitted in the plume and released to the large scale can be deduced as described by Eq. (4).

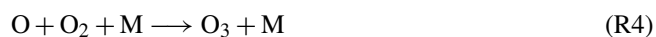
$$\frac{\partial \overline{r_{\text{NO}_x}}}{\partial t} + \langle F_{\text{NO}_x} \rangle = + \frac{1}{\tau} \cdot \overline{r_{\text{LNO}_x}} \cdot \alpha_{\text{NO}_x} + L_{\text{ss}}, \quad (4)$$

where $\overline{r_{\text{NO}_x}}$ is the mixing ratio of NO_x (in ppb) in the model grid, α_{NO_x} is the molecular mass ratio between the air and NO_x species, and L_{SS} is the large-scale sources and sinks (in molecules cm⁻² s⁻¹), such as natural and anthropogenic emissions, photochemical reaction, mixing, and conversion to reservoir species.

We consider a fairly simple chemistry within the plume as described below. The increase in the nitrogen oxide concentration in the upper troposphere leads to ozone production through the reaction of NO with peroxide (HO₂), CH₃O₂, or RO₂ radicals from the OH oxidation as shown by Reaction (R1).



In the case of large NO_x injection by lightning, the NO_x content (~40 ppt in unpolluted atmosphere) becomes close (a few ppb, according to in situ measurements; Dye et al., 2000; Huntrieser et al., 2002) to the surrounding ozone (60 ± 24 ppb) (Jaéglé et al., 1998). The ozone evolution within the plume is described by Reactions (R2)–(R6).



From these equations we can define an O_x family (O_x ≡ O + O₃ + NO₂) where the only net loss of O_x is by reactions between atomic oxygen and NO₂ or O₃. The rate of change of each chemical family is given by Eqs. (5), (6), and (7): (Cariolle et al., 2009).

$$\frac{d([\text{O}] + [\text{O}_3])}{dt} = +k_2 \cdot [\text{NO}_2] - k_3 \cdot [\text{NO}] \cdot [\text{O}_3], \\ - k_5 \cdot [\text{O}] \cdot [\text{NO}_2] - 2 \cdot k_6 \cdot [\text{O}_3] \cdot [\text{O}], \quad (5)$$

$$\frac{d([\text{O}] + [\text{O}_3] + [\text{NO}_2])}{dt} = -2 \cdot k_5 \cdot [\text{O}] \cdot [\text{NO}_2], \\ - 2 \cdot k_6 \cdot [\text{O}_3] \cdot [\text{O}] \quad (6)$$

$$\frac{d([\text{NO}] + [\text{NO}_2])}{dt} = 0, \quad (7)$$

where k_i corresponds to the rate constants for the R_i reactions.

Thus, two processes occur to O₃ in the plume during the daytime. On short timescales O_x is conserved. Lightning emissions of NO in the plume are converted into NO₂, but as NO₂ is in O_x family, there is net conservation of O_x. However, on long timescales O_x can be destroyed through the reaction of O with NO₂ and O₃. Both of these processes need to be considered.

The first regime (regime I) occurs at low concentrations of NO_x (relative to O₃). Under these conditions the Reaction (R5) is slow. There is the rapid equilibrium between NO,

NO₂, and O₃ (Reactions R2, R3, and R4). As a consequence, O₃ is converted into NO₂ and can be restored later after dilution of the plume depending on the balance between NO and NO₂ on a large scale (Cariolle et al., 2009). Overall, O_x is conserved. In this regime emitted NO reacts with the available O₃ until the NO to NO₂ ratio in the plume reaches that in the background. Thus, the impact on the O₃ background concentration is to reduce it by the number of molecules of NO emitted multiplied by the background NO₂ to NO_x ratio. The effect of the first regime on the ozone burden is expressed by Eq. (8).

$$\frac{\partial \overline{r_{\text{O}_3}}}{\partial t} + \langle F_{\text{O}_3} \rangle = -\frac{1}{\tau} \cdot \overline{r_{\text{LNO}_x}} \cdot \alpha_{\text{NO}_x} \cdot \left(\frac{\overline{\text{NO}_2}}{\overline{\text{NO}_x}} - E \right) \cdot \delta + L_{\text{SS}}, \quad (8)$$

where $\overline{r_{\text{O}_3}}$ is the mixing ratio of O₃ (in ppb) in the model grid, E is the $\frac{\text{NO}_2}{\text{NO}_x}$ ratio in the initial emissions, δ is equal to 1 during the day and 0 during the nighttime, and L_{SS} is the sources and sinks of ozone, such as photochemical production, transport from the stratosphere, surface deposition, photolysis reactions, and photochemical destruction.

The second regime (regime II) occurs at high concentrations of NO_x (relative to O₃). Under these conditions the rate of R5 is large. The nonlinear chemical interactions between NO_x and O₃ occur with different rates than in the background atmosphere. To account for this, Cariolle et al. (2009) introduced an effective reaction rate constant (K_{eff}), which is related to the production or the destruction of the odd oxygen (O_x) within the plume. K_{eff} is expressed by Eq. (9).

$$K_{\text{eff}} = \frac{\int_{t_0}^{T_1} \left(\int_{V_p} K \cdot r_{\text{NO}_x}^p \cdot r_{\text{O}_3}^p \cdot dV_p \right) \cdot dt}{\overline{r_{\text{O}_3}} \cdot \int_{t_0}^{T_1} \left(\int_{V_p} r_{\text{NO}_x}^p \cdot dV_p \right) \cdot dt}, \quad (9)$$

where $r_{\text{NO}_x}^p$ and $r_{\text{O}_3}^p$ are the mixing ratios of nitrogen oxides and ozone within the plume, $\overline{r_{\text{O}_3}}$ is the background ozone mixing ratio averaged in the model grid, and K is the rate of NO_x–O₃ reaction within the plume.

The analysis of the chemical reactions related to the two regimes shows that [O₃] ≫ [O] and $k_5 \times [\text{NO}_2]$ is more efficient than $k_6 \times [\text{O}_3]$ as a sink for O_x (Cariolle et al., 2009). Thus, Eq. (6) is simplified to give Eq. (10).

$$\frac{d([\text{O}_3] + [\text{NO}_2])}{dt} = -2 \cdot k_5 \cdot [\text{O}] \cdot [\text{NO}_2] \quad (10)$$

Consequently, K_{eff} can be simplified to Eq. (11).

$$K_{\text{eff}} = \frac{2 \cdot \left(\int^T k_5 \cdot \text{O} \cdot \text{NO}_2 \cdot dt \right)}{(\text{NO}_x \cdot \int^T \text{O}_x \cdot dt)} \quad (11)$$

The calculation of K_{eff} is detailed in Sect. 3.2.4. Considering the two regimes related to the sub-grid plume chemistry, the ozone burden is described by Eq. (12) during the daytime and nighttime. Note that during the nighttime there is no direct

impact on its burden due to the ozone plume chemistry as $\delta = 0$. Only indirect effects are expected from NO_y chemistry.

$$\frac{\partial \overline{r_{O_3}}}{\partial t} + \langle F_{O_3} \rangle = -\frac{1}{\tau} \cdot \overline{r_{LNO_x}} \cdot \alpha_{NO_x} \cdot \left(\frac{\overline{NO_2}}{\overline{NO_x}} - E \right) \cdot \delta - K_{\text{eff}} \cdot \overline{r_{LNO_x}} \cdot \rho \cdot \alpha_{NO_x} \cdot \overline{r_{O_3}} \cdot \delta + L_{\text{ss}} \quad (12)$$

In addition, we consider the conversion of NO_x into HNO₃ within the plume. This conversion takes place in two different ways depending on the day or night atmospheric conditions. During the day, NO₂ reacts primarily with OH to give HNO₃ directly, and it is characterized by the coefficient β_1 , while during the nighttime the conversion of NO_x to HNO₃ occurs mainly through the N₂O₅ formation followed by a heterogeneous hydrolysis reaction, which corresponds to β_2 . In other words, the β coefficients are the molar fractions of NO_x converted to HNO₃ within the plume. These two fractions are unitless.

In summary, the equation system solved on a large scale by the CTM for a lightning NO_x source is detailed by Eqs. (13), (14), and (15).

$$\frac{\partial \overline{r_{NO_x}}}{\partial t} + \langle F_{NO_x} \rangle = +\frac{1}{\tau} \cdot \overline{r_{LNO_x}} \cdot (1 - \beta_1 \cdot \delta - \beta_2 \cdot (1 - \delta)) \cdot \alpha_{NO_x} + L_{\text{ss}}, \quad (13)$$

$$\frac{\partial \overline{r_{HNO_3}}}{\partial t} + \langle F_{HNO_3} \rangle = +\frac{1}{\tau} \cdot \overline{r_{LNO_x}} \cdot (\beta_1 \cdot \delta + \beta_2 \cdot (1 - \delta)) \cdot \alpha_{NO_x} + L_{\text{ss}}, \quad (14)$$

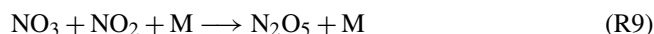
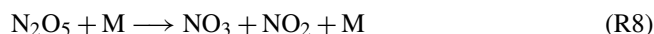
$$\frac{\partial \overline{r_{O_3}}}{\partial t} + \langle F_{O_3} \rangle = -\left(\frac{1}{\tau} \cdot \left(\frac{\overline{NO_2}}{\overline{NO_x}} - E \right) + K_{\text{eff}} \cdot \overline{r_{O_3}} \cdot \rho \right) \cdot \overline{r_{LNO_x}} \cdot \alpha_{NO_x} \cdot \delta + L_{\text{ss}}, \quad (15)$$

where $\overline{r_{NO_x}}$, $\overline{r_{HNO_3}}$, and $\overline{r_{O_3}}$ correspond to the NO_x, HNO₃, and O₃ mixing ratios averaged over the grid cell of the model, respectively.

In this study, the tropospheric chemistry and especially the LNO_x plume chemistry is considered both during the daytime and nighttime since no reactions are initiated during the day. The chemical interactions during the night correspond mainly to the reactions of O₃ and O with NO and NO₂ as well as the NO_x deactivation and the chemistry of the nitrogen reservoir species (here, HNO₃ and N₂O₅) and the nitrate radical (NO₃). NO₃ is the main oxidant in night conditions and is produced from the slow oxidation of NO₂ by O₃ (Reaction R7).

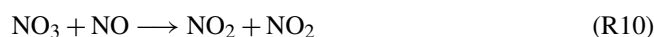


The other dominant source of NO₃ is the destruction of N₂O₅ (Reaction R8), but as N₂O₅ is formed from NO₃ (Reaction R9), the two species act in a coupled manner.



As mentioned previously, N₂O₅ is a determining species for the tropospheric chemistry during the nighttime, allow-

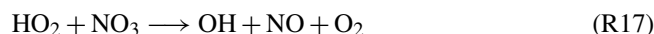
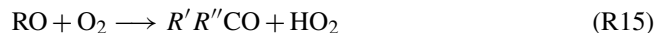
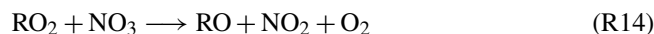
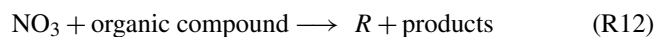
ing the HNO₃ formation by the heterogeneous reaction on the particle surface (aerosols and ice crystals). During the day, NO₃ rapidly undergoes photolysis to produce NO or NO₂. In addition, NO₃ reacts very quickly with NO, which is more concentrated during the daytime than during the nighttime (Reaction R10) but NO₃ is very low during the daytime. However, this reaction can take place during the night, especially for a plume characterized by high NO mixing ratios (like a plume from lightning emissions) which is transported both during the day and at night.



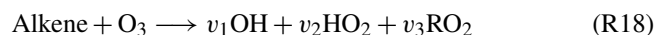
Furthermore, the nitrate radical can potentially react with VOCs. The reaction of the unsaturated hydrocarbons such as isoprene, butenes, and monoterpenes with NO₃ leads to the HNO₃ formation (Monks, 2005) (Reaction R11).



Considering NO₃ reaction with alkenes, an additional mechanism is found initiating a complex chemistry allowing the formation of NO₂ or organic nitrates (Monks, 2005). Finally, NO₃ can initiate VOC oxidation via peroxy radical production (Reaction R12). That way, it can be involved as a chain propagator (Reactions R13 to R17).



The reactions of HO₂ with ozone (R16) or NO₃ (Reaction R17) imply OH production. Also, the reaction of ozone with alkenes allows the formation of OH during the night (Reaction R18) (Aumont, 2005).



Reaction (R18) occurs when ozone concentrations remain sufficiently high in night conditions, in other words for polluted atmosphere.

In this context, we consider different values during the daytime and nighttime for the plume lifetime, the effective reaction rate constant, and the fraction of NO_x conversion into HNO₃ within the plume. Distinguishing day and night chemistry is linked with the fluctuation of the critical r_1 value (below which the sub-grid plume chemistry is negligible), depending on atmospheric conditions. Therefore, if r_1 changes with sunlight, the plume lifetime also changes. Note that except for the β_2 fraction, this night chemistry is not considered by the initial plume approach developed by Carille et al. (2009), which considers NO_x plumes from aircraft exhausts only during the daytime.

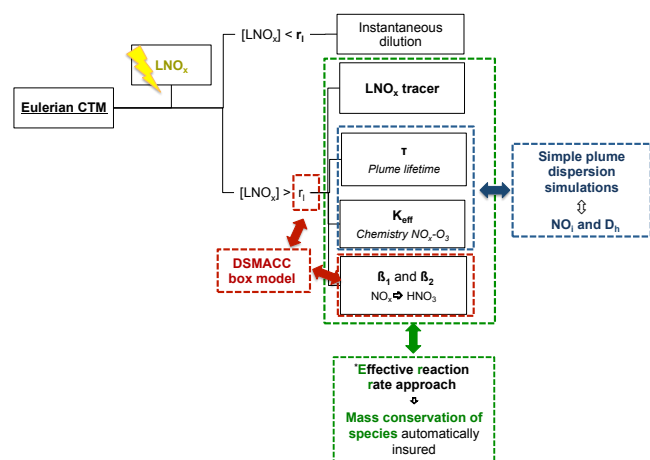


Figure 1. Diagram of the lightning NO_x plume parameterization based on the effective reaction rate approach. The arrows link the parameters to their estimate approach. The red boxes are for the parameters estimated with the DSMACC model and the blue boxes are related to the parameters calculated with the simple plume dispersion model. Finally, the green boxes show the effective reaction rate approach in the GEOS-Chem CTM.

Figure 1 summarizes all elements which define the plume approach and how it has been adapted and implemented into the model.

3.2 Parameter calculations for lightning NO_x emissions

In order to reproduce more accurately the lightning NO_x sub-grid chemistry, some points should be considered: (i) the latitude (NO_x emissions by lightning are higher in the tropics than in the midlatitudes); (ii) the sunlight conditions (day and night), which impact photochemistry and heterogeneous chemistry; (iii) the plume evolution with its own physical characteristics (the lifetime and dispersion properties); and finally (iv) chemical interactions within the plume related to highly elevated NO_x concentrations relative to the background. In the following section, physical and chemical characteristics of the plume associated with a lightning NO_x source have been defined.

3.2.1 Dynamical conditions

The horizontal diffusion coefficient (D_h) is a key parameter of the atmospheric dynamical conditions in determining the dispersion of the lightning NO_x plume. D_h is used as the dispersion constraint for the simple plume dispersion simulations carried out in order to estimate the plume lifetime and the effective reaction rate constant. The diffusion coefficient was determined in two different ways. A first estimate of the horizontal diffusion was performed by running the 3-D mesoscale Meso-NH model. Then, the D_h coefficient was calculated using in situ measurements in a thunderstorm anvil.

The Meso-NH mesoscale model was used (see Sect. 2.2) to investigate D_h . A simple convective cell forced by a warm bubble and initialized by a radiosounding at the simulation start was run as an ideal case. Simulations were realized for a domain of 24 km in the two horizontal directions, and the grid horizontal resolution is $\Delta x = \Delta y = 1$ km and $\Delta z = 500$ m. The convective cell is located at 43.29° N latitude and 0° longitude (Klemp and Wilhelmson, 1978). Simulations of 6 h were performed, allowing the complete development and the dissipation of the convective cell. D_h was calculated within the anvil using the mixing length diagnostic variable, hereafter denoted L , as described by Eq. (16) (Cuxart et al., 1999).

$$D_h = \frac{2}{3} \times \frac{L}{4} \times \exp\left(\frac{1}{2}\right) \quad (16)$$

At the mature stage of the cell, D_h was calculated as $100 \text{ m}^2 \text{ s}^{-1}$ within the upper levels of the convective cell (i.e., in the anvil, defined empirically).

In addition to the modeling estimate, we used in situ measurements to calculate D_h . Turbulence measurements were performed by a B-757 commercial aircraft along a flight from the west of Kansas to the north of Missouri and corresponding to a trajectory of more than 500 km (Trier and Sharman, 2008). These in situ measurements were carried out from 07:00 to 10:00 UTC on 17 June 2005, during the development of a mesoscale convective system (MCS). This MCS is associated with a turbulence event characterized by the measurement of the atmospheric eddy dissipation rate (ϵ) and the turbulence kinetic energy (TKE) above and within the cloud anvil. The higher values of ϵ ($\epsilon^{1/3} \sim 0.4 \text{ m}^{2/3} \text{ s}^{-1}$) were recorded between 11.3 and 11.6 km altitude, corresponding to the cloud anvil levels. In addition, for this MCS, the TKE was about $1 \text{ m}^2 \text{ s}^{-2}$ at the locations of the highest ϵ values.

According to these observations, the turbulent diffusivity (Eq. 17) was estimated above the anvil of the MCS (http://www.ral.ucar.edu/projects/turb_char/), such that $D_h > 0.1 \text{ m}^2 \text{ s}^{-2}$. Then, D_h was calculated within the anvil such that $D_h = 15 \text{ m}^2 \text{ s}^{-1}$ using the same formulation (Eq. 17). This last estimate seems to be the most common value compared to the diffusion coefficient value of $20 \text{ m}^2 \text{ s}^{-1}$ used by Cariolle et al. (2009), close to the tropopause level and the D_h value calculated for contrails ($15 \text{ m}^2 \text{ s}^{-1}$) in the upper troposphere (Knollenberg, 1972).

$$D_h = \frac{(\text{TKE})^2}{\epsilon} \quad (17)$$

The D_h estimate using the Meso-NH model is high compared to the results from measurements, corresponds to the upper limit of the calculated diffusion coefficients, and may be associated with the turbulence in the convective cloud. However, it is important to note that usually most numerical simulations are performed with 1-D turbulence models. What is interesting in the use of Meso-NH in this study is that the 3-D

turbulence is solved. This simulation provides an additional estimate of D_h , allowing a comparison with the calculation from in situ measurements. Moreover, studies on the diffusivity in cloud anvils are uncommon. It is necessary to conduct additional work in the future on that issue, again constrained with new in situ measurements of the atmospheric turbulence in the anvil.

It is important to note that the 3-D turbulence is not solved online in the GEOS-Chem model because of the fine scale characterizing this process but is prescribed by the GEOS-5 met fields. Therefore, the global variability of D_h is not calculated by the CTM, and it is beyond the scope of this study.

In order to cover all horizontal diffusivity estimates discussed in this section, values of 0.1, 15, and 100 m² s⁻¹ were used. The horizontal coefficient is constant for all lightning NO_x plumes which are considered in the GEOS-Chem model. Hereafter, the results are detailed for the central value $D_h = 15$ m² s⁻¹. Sensitivity tests depending on the uncertainty associated with the parameter estimate are performed and presented later in Sect. 4.3.

3.2.2 The NO_x critical plume content (r_1)

The r_1 critical value is the NO_x mixing ratio within the undiluted phase of the plume below which the nonlinear chemistry can be neglected (Sect. 3.1). It has been estimated using the 0-D DSMACC box model (Sect. 2.2). Initial conditions for simulations carried out with the DSMACC box model are from outputs of the GEOS-Chem model. In particular, initial atmospheric parameters and atmospheric background concentrations of species correspond to the average of the GEOS-Chem outputs (i) from 8 to 11 km, (ii) for two latitude regions (tropics and midlatitudes), and (iii) for the year 2006 (Table 1). The altitude range refers to the detrainment region estimated by GEOS-Chem using the GEOS-5 met fields (Sect. 2.1) both in the tropics and in the midlatitudes. Note that this range can vary depending on the met fields and the convection parameterization. In addition, the LNO_x plume parameterization should have an impact outside of this altitude range, mainly between 6 and 12 km, but to a lesser extent.

In order to focus on chemistry interactions only between chemical species of interest and on removing the mixing influence and sunlight fluctuations, short simulations (i.e., 1 h each) were run with the DSMACC model. The effects of the day or night conditions were carefully considered, carrying out separate simulations during the daytime and nighttime. Simulations were run for a large range of initial NO mixing ratios from 0.01 ppb to 1 ppm. The r_1 value is defined from the NO value, for which the $\frac{\partial O_x}{\partial t}$ trend is perturbed. In other words, r_1 is associated with the second derivative of O_x, i.e., the curve optimums on Fig. 2. The r_1 threshold was defined to be 0.1 and 0.25 ppb during the day and at night for mid-

latitudes and 0.1 and 0.75 ppb during the day and at night in the tropics (Fig. 2).

Note that the midlatitudes and the tropics were separated because of the large differences in LNO_x emissions between the two regions in terms of the number of flashes in a particular convective cell, which is higher in the tropics according to the LIS-OTD climatologies (Christian et al., 2003). This last point is important for the plume lifetime estimate detailed in the following section.

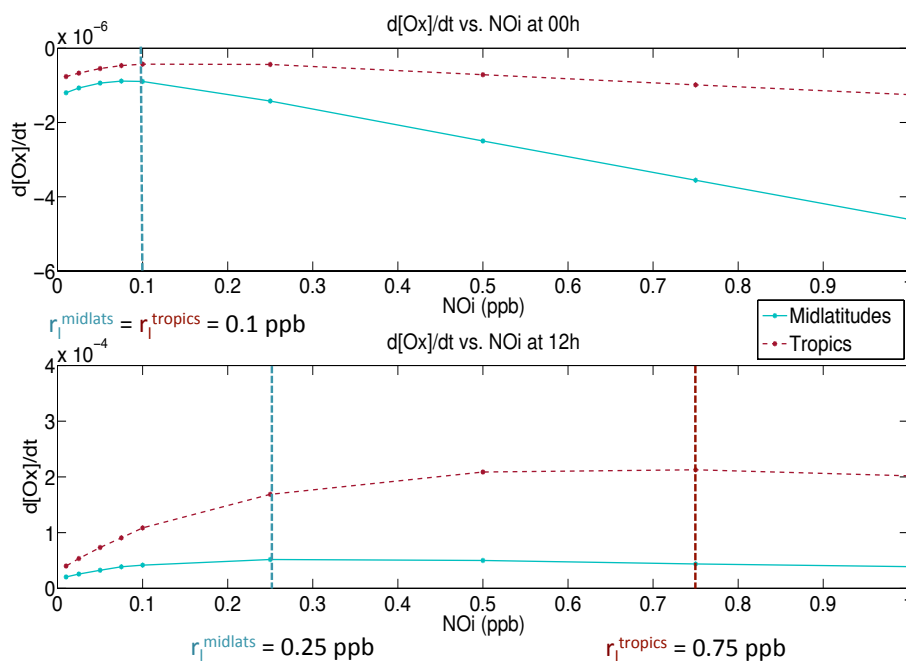
3.2.3 The plume lifetime τ

The plume lifetime (τ) depends directly on (i) the initial NO pulse from lightning emissions, (ii) the r_1 critical value, and (iii) the diffusion properties of the atmosphere. The plume lifetime also depends on the initial size of the plume. Here we use a width of 500 m in order to include an ensemble of spikes on the cloud scale (i.e., each plume is defined from several electrical discharges on a convective cell scale). τ is crucial for the physical description of the NO_x plumes, and it has been computed by carrying out dispersion simulations of a simple plume assumed to be cylindrical. In this model, the standard atmospheric conditions are represented by temperature, pressure, and species concentrations of the background atmosphere, which are similar to the initial conditions used for the DSMACC simulations. As a reminder, initial conditions are from GEOS-Chem outputs averaged (i) from 8 to 11 km, (ii) for two latitude regions (tropics and midlatitudes), and (iii) for the year 2006 (Table 1). Simulations are initialized by an NO pulse from lightning emissions (hereafter denoted NO_i), and the plume dispersion depends on the D_h value estimated in Sect. 3.2.1.

The initial tracer concentration NO_i related to lightning NO emissions on the scale of a convective cell (gathering several flashes together) in the midlatitudes was defined according to previous aircraft measurement campaigns. In particular, the STERAO (Stratospheric-Tropospheric experiment: radiation, aerosols, and ozone) campaign recorded NO spikes of a magnitude from 1 to 10 ppb related to lightning activity in thunderstorms and occurring from 9 to 10 July 1996 over northern Colorado (Dye et al., 2000; Stith et al., 1999). Lange et al. (2001) measured NO spikes of 3.5 ppb during the STREAM (Stratosphere-Troposphere Experiment by Aircraft Measurements) campaign associated with a matured storm over Ontario. Several peaks of NO mixing ratios from 0.7 to 6 ppb were also observed during EULINOX (European Lightning Nitrogen Oxides Project; Huntrieser et al., 2002) over Germany in July 1998. The LINOX (Lightning NOx) aircraft campaign recorded NO spikes from 0.75 to 1.25 ppb (Huntrieser et al., 1998) related to thunderstorms over Europe on 30 July 1996. From these studies, the NO concentration associated with the electrical activity in thunderstorms occurring over the midlatitudes was determined as NO_i^{mean, Midlats} = 3.4 ppb (NO_i^{min, Midlats} = 0.7 ppb and NO_i^{max, Midlats} = 10 ppb). Because there are much fewer

Table 1. The initial atmospheric parameters and background concentrations of chemical species from GEOS-Chem outputs for the DSMACC box model simulations.

| | Temp. | Press. | O ₃ | NO | NO ₂ | HNO ₃ | HNO ₄ | PAN | N ₂ O ₅ | CO |
|--------------|-------|-----------------|-------------------------------|-------------------|--------------------------------|-------------------------------|-------------------------------|---------------------------------|---------------------------------|-------|
| Units | (K) | (hPa) | (ppb) | (ppb) | (ppb) | (ppb) | (ppb) | (ppb) | (ppt) | (ppb) |
| Midlatitudes | 228 | 313 | 67 | 0.04 | 0.01 | 0.15 | 0.02 | 0.1 | 2 | 94 |
| Tropics | 240 | 313 | 26 | 0.03 | 0.003 | 0.02 | 0.006 | 0.03 | 2.3 | 93 |
| | OH | HO ₂ | H ₂ O ₂ | CH ₂ O | CH ₄ O ₂ | C ₃ H ₈ | C ₅ H ₈ | C ₂ H ₄ O | C ₃ H ₆ O | |
| Units | (ppb) | (ppt) | (ppt) | (ppb) | (ppb) | (ppb) | (ppb) | (ppb) | (ppb) | |
| Midlatitudes | 0.2 | 4 | 0.4 | 0.06 | 0.1 | 0.47 | 0 | 7.5 | 4 | |
| Tropics | 0.06 | 6 | 0.34 | 0.03 | 0.17 | 0.13 | 7.5 | 7.5 | 4 | |

**Figure 2.** r_1 critical value and odd oxygen trends from DSMACC box model simulations for midlatitudes (solid line) and tropics (dotted line) at midnight (upper panel) and at midday (bottom panel).

LNO_x measurements in the tropics and in order to be consistent with the LNO_x emissions defined in the GEOS-Chem model, the ratio $R_{\text{LNO}_x} = \frac{\text{LNO}_x^{\text{Midlatitudes}}}{\text{LNO}_x^{\text{Tropics}}}$ was defined as in the CTM. During the year 2006, the relative midlatitude and tropics LNO_x contribution was about $R_{\text{LNO}_x} = 0.33$. This result is in agreement with higher LNO_x emissions in these regions rather than in the midlatitudes. The value of the NO mixing ratio injected by lightning into the tropics was estimated as $\text{NO}_i^{\text{mean, Tropics}} = 10.2$ ppb ($\text{NO}_i^{\text{min, Tropics}} = 2.8$ ppb and $\text{NO}_i^{\text{max, Tropics}} = 29.7$ ppb).

Once the NO_i estimate was completed, the calculation of the plume lifetime was achieved using the detailed formulation given in Sect. 3.1.1. The results for τ are summarized in Table 2. Hereafter, the results are detailed for $\text{NO}_i^{\text{mean}}$ in Sect. 4, and sensitivity tests are carried out using all NO_i

values for the midlatitudes and the tropics (Sect. 5). Model calculations for $\text{NO}_i^{\text{mean}}$ and $D_h = 15 \text{ m}^2 \text{ s}^{-1}$ provide a minimum plume lifetime of 3 (6) h for the midlatitudes and maximum plume lifetime of 9 (21.3) h for the tropics during the daytime (nighttime).

3.2.4 The effective reaction rate constant (K_{eff})

The nonlinear chemistry within the plume has been considered in calculating the effective reaction rate constant (K_{eff}), which is used to compute the formation of the secondary species (O_x and HNO₃) within the plume. K_{eff} is associated with the evolution of odd oxygen depending on the O and O₃ reactions with NO₂ and NO, and also on the NO_x activation (day) or deactivation (night) with the HNO₃, N₂O₅, and PAN chemistry. Note that in the case of lightning emissions,

Table 2. The plume lifetime τ (hours) calculated for midlatitudes and tropics depending on the initial NO mixing ratio injected by lightning emissions (NO_i , ppb) and the horizontal diffusion coefficient (D_h , $\text{m}^2 \text{s}^{-1}$) for day (upper part of table) and night conditions (bottom part of table).

| Day | | | | | | |
|--------------------------------------------|---------------------|------|------|---------|------|------|
| τ (hours) | Midlatitudes | | | Tropics | | |
| | NO_i (ppb) | 0.7 | 3.4 | 10 | 2.8 | 10 |
| $D_h = 0.1$ ($\text{m}^2 \text{s}^{-1}$) | 1.55 | 8.14 | 23.9 | 4.40 | 23.1 | 67.9 |
| $D_h = 15$ ($\text{m}^2 \text{s}^{-1}$) | 0.1 | 3.17 | 18.6 | 0.27 | 8.90 | 52.8 |
| $D_h = 100$ ($\text{m}^2 \text{s}^{-1}$) | 0.01 | 0.47 | 4.17 | 0.04 | 1.32 | 11.7 |
| Night | | | | | | |
| τ (hours) | Midlatitudes | | | Tropics | | |
| | NO_i (ppb) | 0.7 | 3.4 | 10 | 2.8 | 10 |
| $D_h = 0.1$ ($\text{m}^2 \text{s}^{-1}$) | 1.62 | 8.19 | 24.1 | 4.74 | 23.4 | 68.5 |
| $D_h = 15$ ($\text{m}^2 \text{s}^{-1}$) | 0.31 | 6.19 | 22 | 2.77 | 21.3 | 66.4 |
| $D_h = 100$ ($\text{m}^2 \text{s}^{-1}$) | 0.05 | 1.23 | 10.6 | 0.43 | 10.5 | 55.4 |

other species like VOCs, HO_x, and H₂O may be uplifted into the convective region. However, we assumed that the OPE is mainly controlled by NO_x in the upper troposphere, as previously showed by Sauvage et al. (2007b). Therefore, the K_{eff} calculation is here mainly dependent on NO_x content. Future studies should try to investigate this issue for lightning emissions mixed with strong surface emissions in order to sharpen our parameterization.

K_{eff} is calculated according to Eq. (11) of Sect. 3.1.2 using the same simple plume dispersion simulations as those carried out to define the plume lifetime (Sect. 3.2.3).

Results for K_{eff} are summarized in Table 3. Model calculations using $\text{NO}_i^{\text{mean}}$ and $D_h = 15 \text{ m}^2 \text{ s}^{-1}$ give a K_{eff} value of $5.49 \times 10^{-19} \text{ molecules}^{-1} \text{ s}^{-1} \text{ cm}^3$ ($4.55 \times 10^{-19} \text{ molecules}^{-1} \text{ s}^{-1} \text{ cm}^3$) in the midlatitudes and $3.64 \times 10^{-19} \text{ molecules}^{-1} \text{ s}^{-1} \text{ cm}^3$ ($2.98 \times 10^{-19} \text{ molecules}^{-1} \text{ s}^{-1} \text{ cm}^3$) in the tropics during the daytime (during the nighttime).

Our K_{eff} estimates are smaller than those calculated by Cariolle et al. (2009) for the plume chemistry related to aircraft exhausts. In this previous work, K_{eff} varies from 1.0 to $4.2 \times 10^{-18} \text{ molecules}^{-1} \text{ s}^{-1} \text{ cm}^3$, with a mean value close to $3 \times 10^{-18} \text{ molecules}^{-1} \text{ s}^{-1} \text{ cm}^3$ depending on the NO_x loading. The very low value for K_{eff} indicates that the plume parameterization implies a delay in the production of ozone on a large scale rather than its destruction within the plume.

3.2.5 The fractions of NO_x conversion to HNO₃ (β_1 and β_2)

The fractions β_1 and β_2 represent the NO_x conversion to HNO₃ within the plume during the daytime and nighttime, respectively. They were computed using the DSMACC box model.

The β_1 coefficient was calculated for day conditions depending mainly on the OH concentration. The conversion of NO_x into HNO₃ during the nighttime (β_2 coefficient) is related to the heterogeneous reaction of N₂O₅ and so depends on particle (aerosols and ice crystals) concentration and particles' lifetime. This is directly linked with the surface density and the radius of particles in the anvil region of thunderstorms, which is highly uncertain. We defined these values using in situ measurements. The surface area (S_T) and the radius (R) for aerosols are defined such that $S_T = 0.28 \text{ m}^{-1}$ and $R = 1 \mu\text{m}^{-1}$ (Huntrieser et al., 2002); for ice, these are $S_T = 0.03 \text{ m}^{-1}$ and $R = 30 \mu\text{m}^{-1}$ (Knollenberg et al., 1993). In addition, the reaction probabilities of NO_x on aerosols and ice crystals $\gamma_{\text{N}_2\text{O}_5}^{\text{aerosols}} = 0.02$ (Evans and Jacob, 2005) and $\gamma_{\text{N}_2\text{O}_5}^{\text{ice}} = 0.03$ (Sander et al., 2006), respectively, were used for our box model simulations. These values correspond to the probability that an N₂O₅ molecule impacting an aerosol or an ice crystal surface reacted. The results for β_1 and β_2 coefficients are summarized in Table 4.

The estimate of the β_1 fraction does not show significant variation, neither between latitudes regions nor depending on NO_i. The minimum β_1 value is 1.34×10^{-4} for the tropical regions and NO_i^{min} , and the maximum β_1 value is 1.88×10^{-4} for the midlatitudes and NO_i^{max} . The study of production and destruction rates for day conditions taking into account all reactions pathways (not shown here) demonstrates that the production of HNO₃ during the day is mainly determined by the reaction of NO₃ with formaldehyde (HCHO) and acetaldehyde (CH₃CHO). Surprisingly, the HNO₃ formation via the NO₂+OH reaction seems to be less efficient. This result may be explained by the low initial concentrations of OH used for the DSMACC simulations, and it is in agreement with the small β_1 values. The averaged β_2 coefficient is higher by a factor 10 compared to β_1 with a minimum value of 0.24×10^{-3} in the tropics for NO_i^{max} and a maximum estimate of 14.4×10^{-3} in the midlatitudes for NO_i^{min} . The analysis of the production and the destruction rates for night conditions taking into account all reaction pathways shows that the predominant reaction in the HNO₃ evolution is N₂O₅+H₂O (or the heterogeneous reaction on the aerosol and ice crystal surfaces).

4 Results: CTM simulations

In this section, the effects of the lightning NO_x plume parameterization, i.e., the influence of the sub-grid processes related to lightning emissions, on the NO_x and O₃ tropospheric distributions on a large scale are evaluated. Then, the parameterization sensitivity to the initial NO mixing ratio injected by lightning (NO_i) and the D_h , β_1 , and β_2 coefficients are analyzed to quantify the variability of the results regarding the plume-in-grid parameter calculations.

Table 3. The effective reaction rate constant K_{eff} (10^{-19} molecules⁻¹ s⁻¹ cm³) in the midlatitudes and tropics depending on the initial NO mixing ratio injected by lightning emissions (NO_i , ppb) and the horizontal diffusion coefficient (D_h , m² s⁻¹) for day (upper part of table) and night conditions (bottom part of table).

| K_{eff} (10^{-19} molecules ⁻¹ s ⁻¹ cm ³) | Day | | | | | |
|-----------------------------------------------------------------------------------------|--------------|------|------|---------|------|------|
| | Midlatitudes | | | Tropics | | |
| NO_i (ppb) | 0.7 | 3.4 | 10 | 2.8 | 10 | 29.7 |
| $D_h = 0.1$ (m ² s ⁻¹) | 1.28 | 1.24 | 1.51 | 0.77 | 1.2 | 1.83 |
| $D_h = 15$ (m ² s ⁻¹) | 8.44 | 5.49 | 5.43 | 7.79 | 3.64 | 4.13 |
| $D_h = 100$ (m ² s ⁻¹) | 12.1 | 16.4 | 14.4 | 23 | 19.8 | 13 |
| K_{eff} (10^{-19} molecules ⁻¹ s ⁻¹ cm ³) | Night | | | | | |
| | Midlatitudes | | | Tropics | | |
| NO_i (ppb) | 0.7 | 3.4 | 10 | 2.8 | 10 | 29.7 |
| $D_h = 0.1$ (m ² s ⁻¹) | 1.28 | 1.24 | 1.51 | 0.77 | 1.10 | 1.83 |
| $D_h = 15$ (m ² s ⁻¹) | 4.84 | 4.55 | 5.43 | 2.3 | 2.98 | 4.13 |
| $D_h = 100$ (m ² s ⁻¹) | 7.36 | 8.39 | 6.73 | 6.45 | 3.94 | 5.16 |

Table 4. The fractions of NO_x conversion into HNO₃ within the plume (β_1 and β_2) in the midlatitudes and tropics depending on the initial NO mixing ratio injected by lightning emissions (NO_i , ppb) and on particles for day (upper part of table) and night conditions (bottom part of table).

| β_1 (10^{-4}) | Day | | | | | |
|-------------------------|--------------|------|------|---------|------|------|
| | Midlatitudes | | | Tropics | | |
| NO_i (ppb) | 0.7 | 3.4 | 10 | 2.8 | 10 | 29.7 |
| Aerosols | 2.53 | 3.34 | 3.45 | 2.51 | 2.95 | 2.6 |
| Ice | 0.23 | 0.3 | 0.3 | 0.2 | 0.23 | 0.3 |
| Mean | 1.38 | 1.8 | 1.88 | 1.34 | 1.59 | 1.47 |
| β_2 (10^{-3}) | Night | | | | | |
| | Midlatitudes | | | Tropics | | |
| NO_i (ppb) | 0.7 | 3.4 | 10 | 2.8 | 10 | 29.7 |
| Aerosols | 14.3 | 9.89 | 8 | 4.9 | 1.69 | 0.24 |
| Ice | 14.4 | 9.96 | 8.06 | 4.89 | 1.70 | 0.24 |
| Mean | 14.4 | 9.92 | 8.03 | 4.88 | 1.7 | 0.24 |

4.1 Implementation of the LNO_x plume parameterization

The implementation of the lightning NO_x plume parameterization into the GEOS-Chem model requires specifying the system of continuity equations related to the plume chemistry solved on a large scale by the model (Sect. 3.1.2, Eqs. 13, 14, and 15). Lightning NO_x emissions calculated in each grid box (in molecules cm⁻² s⁻¹) by the model are directly used to compute the injection rate I (s⁻¹) of NO at each chemical time step of the simulation. Then, we consider that $\alpha_{\text{NO}_x} = 1$ in order to represent the mixing ratio of the undiluted fraction of NO_x by the tracer (r_{LNO_x}). Furthermore, lightning produces negligible quantities of NO₂ relative to NO, and therefore E is 0 in Eq. (15). Finally, the ratio $\overline{\text{NO}_2/\text{NO}_x}$ is the

relative balance between NO and NO₂ in the diluted phase on a large scale reproduced by the model.

4.2 Impact of LNO_x emissions on the NO_x and O₃ distributions

We perform a spin-up of 6 months (from July 2005 to January 2006) in order to obtain a steady state in the model after activation of the plume parameterization. Then, simulations were run for the entire year 2006. The transport and the convection time steps are 15 min and the emissions and the chemical time steps are 30 min.

In the following, “standard simulation” refers to a simulation with standard lightning NO_x emissions, i.e., those instantaneously diluted in a grid cell, while “modified simulation” refers to a simulation considering the plume parameterization and then the sub-grid chemistry. Note that the modified simulation was run using mean values for the initial NO mixing ratio ($\text{NO}_i^{\text{mean, Midlats}} = 3.4$ ppb and $\text{NO}_i^{\text{mean, Tropics}} = 10.2$ ppb) and $D_h = 15$ m² s⁻¹. The base case (BC) experiment corresponds to the standard simulation minus the standard simulation without lightning NO_x emissions. The P1 experiment corresponds to the modified simulation minus the standard simulation without lightning NO_x emissions. The P2 experiment is the same as the P1 experiment but without considering the nitrification mechanism in the modified simulation (i.e., $\beta_1 = \beta_2 = 0$). In addition, sensitivity tests were performed for P1 defined by the modified simulation using the minimum and the maximum values for D_h , NO_i , and the β_1 and β_2 coefficients. All experiments are summarized in Table 5.

Lightning emissions rates and the associated LNO_x tracer distributions are first discussed; then the effects of the implementation of the plume parameterization (P1) compared to

Table 5. Values of the parameters for the plume parameterization corresponding to the experiments P1 and P2.

| Parameters | Experiments | | | | | | | | | | | | |
|-----------------------------------------|-------------|------|------|-----|------|------|-----|------|------|------|-----|------|-----|
| | P1 | | | | | P2 | | | | | | | |
| D_h (m ² s ⁻¹) | 0.1 | | | 15 | | | 100 | | | 15 | | | |
| NO _i (ppb) | Min | Mean | Max | Min | Mean | Max | Min | Mean | Max | Mean | | | |
| Midlatitudes | 0.7 | 3.4 | 10 | 0.7 | 3.4 | 10 | 0.7 | 3.4 | 10 | 3.4 | | | |
| Tropics | 2.8 | 10.2 | 29.7 | 2.8 | 10.2 | 29.7 | 2.8 | 10.2 | 29.7 | 10.2 | | | |
| β_1 | Mean | | | | | 0 | | | | | Min | Mean | Max |
| β_2 | Mean | | | | | 0 | | | | | Min | Mean | Max |

the experiment without the plume-in-grid development (BC case) are presented.

4.2.1 Lightning emissions and LNO_x tracer distributions

Figure 3 displays the geographical distributions of the 9 km lightning NO_x emissions (a), the related LNO_x tracer distributions (b), and the LNO_x tracer zonal average (c) in January (top panels) and in July (bottom panels), reproduced by the CTM from the P1 experiment. These results are shown for an approximate detrainment level (9 km altitude) where the detrainment of LNO_x is the largest. In January, the highest emissions of NO_x from lightning ($4\text{--}6 \times 10^9$ molecules cm⁻² s⁻¹) are located in the Southern Hemisphere around the tropics over west Australia and central-southern Africa. Also, the model gives low LNO_x emissions ($< 3 \times 10^9$ molecules cm⁻² s⁻¹) over South America and North America, especially over the Gulf of Mexico. In July, the highest LNO_x emissions ($4\text{--}6 \times 10^9$ molecules cm⁻² s⁻¹) are calculated in the Northern Hemisphere over North America, the north of India, central Africa, and the Sahel. In addition, LNO_x emissions are modeled over Europe and over east Asia, but to a lesser extent ($< 2 \times 10^9$ molecules cm⁻² s⁻¹).

The lightning NO_x tracer introduced into the model represents the lightning NO_x emissions affected by the transport and the exponential decay depending on the plume lifetime. Figure 3 shows that the tracer distribution is consistent with the lightning NO_x emissions. However, it is important to note that the plume lifetime is a key factor in the evolution of the LNO_x tracer mixing ratio. A long plume lifetime (several hours to several days) allows the intercontinental transport of LNO_x plumes. The representation of the sub-grid chemistry and the transport of the nonlinear chemistry effects related to the plume consideration becomes important for the chemistry of the regions located far downwind from source regions. The plume lifetime depends on the latitude because of the different background chemical concentrations and the different amount of NO_x emitted from lightning in the tropics and in the midlatitudes. In addition, as mentioned before,

we consider the influence of day and night conditions on the plume lifetime estimate.

According to its preliminary calculation (Sect. 3.2.3), the plume lifetime is longer in the tropics (9 and 21.3 h for day and night conditions, respectively) than in the midlatitudes (3 and 6 h, for day and night conditions, respectively). So, the LNO_x tracer is characterized by a shorter lifetime as a plume over North America than over central Africa and around the Sahel, while the model simulated fewer emissions over these regions, especially in summer. In boreal winter, the mixing ratio of the lightning NO_x tracer calculated by the model is about 0.21 ppb over central and southern Africa, 0.18 ppb over west Australia and 0.11 ppb over South America. In summer, the tracer mixing ratio is simulated as 0.21, 0.32, and 0.16 ppb over central Africa, northern India, and North America, respectively. The lightning NO_x tracer is produced at altitudes where lightning NO_x is calculated and detrained (in the upper troposphere between ~ 500 and 300 hPa) as shown in Fig. 3c.

4.2.2 Impact of lightning on NO_x and O₃ distributions with the plume parameterization

The difference between the P1 and BC experiments (P3) was calculated in order to quantify the changes in NO_x and O₃ mixing ratios on the large scale implied by the implementation of the plume-in-grid parameterization in GEOS-Chem. Figures 4 and 5 display the geographical distributions of the NO_x, HNO₃, PAN, and O₃ absolute changes (in ppb) in January and in July, respectively. The 9 km altitude level was chosen because of the most significant variations at this altitude compared to the rest of the troposphere.

In boreal winter, LNO_x plume chemistry leads to a maximum decrease on a large scale over regions of emissions of 120 ppt for NO_x and a decrease of 68 ppt for HNO₃ and 16 ppt for PAN over central and southern Africa. These variations are associated with a maximum O₃ decrease of 2.8 ppb over regions of emissions. A similar NO_x, HNO₃, PAN, and O₃ reduction is obtained in other areas of high LNO_x emissions (i.e., over west Australia and South America). Downwind of LNO_x emissions, the opposite effect is observed for NO_x and HNO₃ species, with a maximum increase of 40 ppt

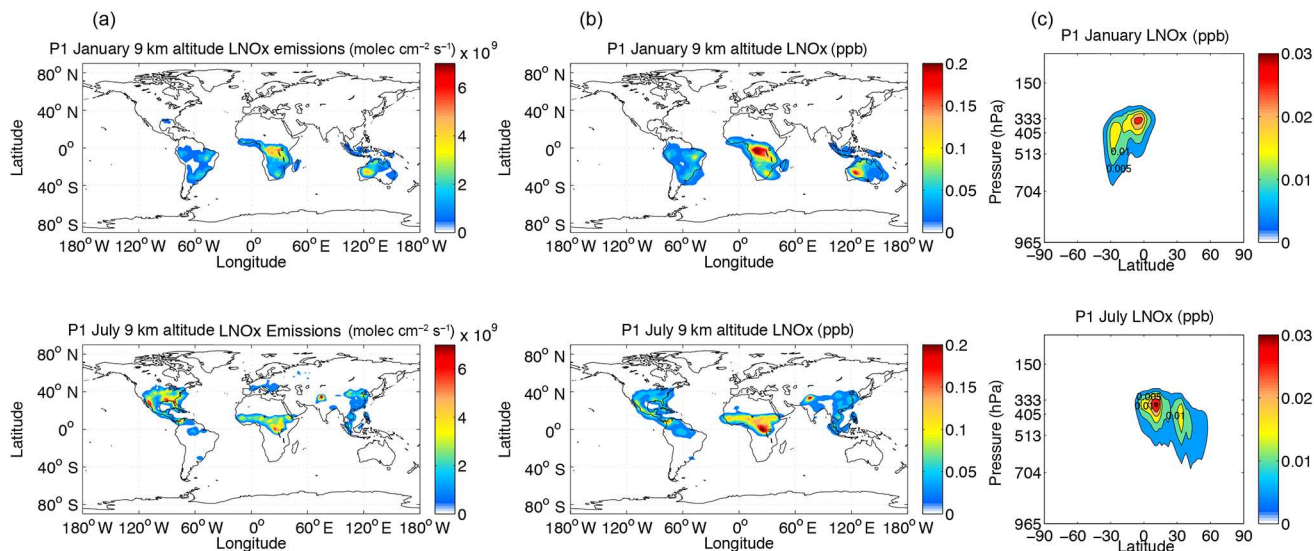


Figure 3. Geographical distributions at 9 km altitude of lightning NO_x emissions (left column, **a**), the geographical distributions of the related LNO_x tracer (in ppb; middle column, **b**), and the zonal average of the LNO_x tracer (in ppb; right column, **c**) for January (top) and July (bottom). Experiment P1, using τ and K_{eff} determined with $D_h = 15 \text{ m}^2 \text{ s}^{-1}$ and $\text{NO}_i^{\text{mean}}$ and performed with the GEOS-Chem model.

for NO_x and 13.5 ppt for HNO₃ observed over the South Atlantic and Indian Ocean. Generally, PAN still decreases over oceans but to a lesser extent compared to regions of LNO_x emissions, with a maximum reduction of 9 ppt. The O₃ response is a maximum increase of 1.13 ppb around the area where the transport is effective and especially over the oceans. In summer, maximum decreases of 140 ppt for NO_x, 60 ppt for HNO₃, and 24 ppt for PAN are calculated by the CTM, leading to a maximum O₃ decrease of 2.4 ppb over central Africa (reduction is also observed over North America and northern India). Downwind of lightning emissions, an increase in NO_x and HNO₃ is observed, with a maximum value of 30 ppt and 38 ppt, respectively. The PAN reservoir species also still decrease slightly downwind, with 2 ppt changes. Finally, this leads to a maximum O₃ increase of 0.7 ppb.

Note that the production of PAN is limited by the supply of NO_x or non-methane volatile organic compounds (NMVOCs). Above continental lightning sources regions, NMVOCs are uplifted by deep convection but with lower NO_x due to the activation of the plume parameterization. This implies a less efficient PAN production in these regions. Downwind of lightning source regions (oceanic regions), NO_x increases because of the LNO_x transport in the plume, but there are less NMVOCs available to produce PAN. Therefore, both in regions of LNO_x emissions and downwind, PAN production is limited, leading to overall lower PAN mixing ratios on a large scale in the P1 experiment. However, this a more nuanced view of this may be obtained by considering the PAN chemistry in future studies using a similar LNO_x plume parameterization and by intro-

ducing the PAN and CH₃C(O)OO continuity equations and a new term to consider the fraction of NO_x converted to PAN within the plume. This should enable PAN production during plume transport, which is inhibited in the current version.

In order to provide a full overview of the effects of the plume parameterization, the relative difference between the P1 and BC experiments (i.e., P3/BC) was calculated integrated throughout the troposphere. Figures 6 and 7 show the zonal average of NO_x (upper panels) and O₃ (bottom panels) relative changes (in %) integrated throughout the troposphere for the regions of interest for January and July. During boreal winter, the highest NO_x (O₃) decreases of 10 % (5 %) in west Australia; then 20 % (6 %) in central Africa are calculated. These negative variations are mainly calculated between 400 hPa and the tropopause level for NO_x and ozone. South America is characterized by a decrease of 20 % in the nitrogen oxides and 1 % in ozone. Over this region, variations are significant in the entire troposphere for both species. In contrast to the continent decrease, an NO_x increase is observed over the major part of the South Atlantic and the Indian Ocean, with a 14 and 20 % maximum, respectively. O₃ responds with an increase of 1 % near the tropopause, and it becomes higher by about 4 % close to the surface. In summer, there is an NO_x (O₃) decrease of 25 % (8 %) over central Africa, 20 % (2 %) over northern India, and 5 % (0.5 %) over North America. Also, the South Atlantic and Indian Ocean (located downwind of lightning NO_x emissions) are characterized by a maximum increase of 18 % for NO_x and 2 % for O₃.

As a result, the sub-grid chemistry associated with the LNO_x emissions implies (i) a decrease in the nitrogen oxides

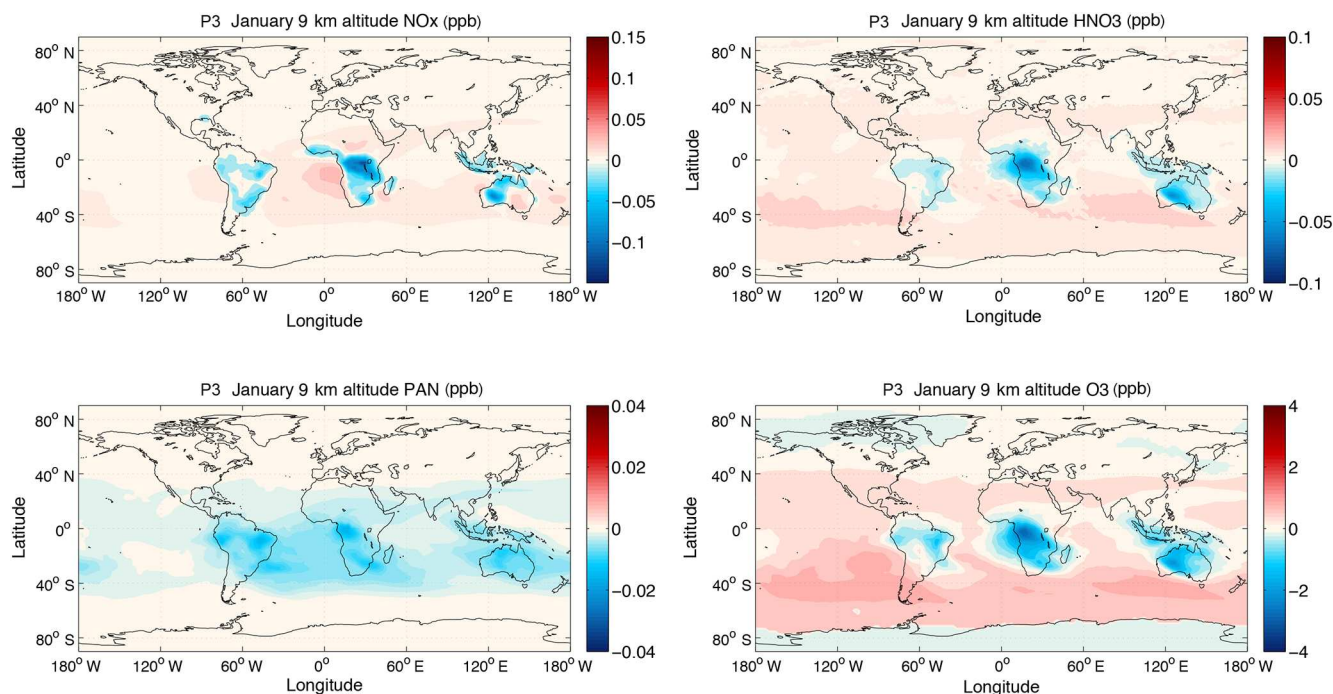


Figure 4. Geographical distributions of NO_x, HNO₃, PAN, and O₃ variations (in ppb) at 9 km altitude for January from the absolute difference (P3) between P1 and BC experiments. P1 was performed using τ and K_{eff} determined with $D_h = 15 \text{ m}^2 \text{ s}^{-1}$ and $\text{NO}_i^{\text{mean}}$ with GEOS-Chem.

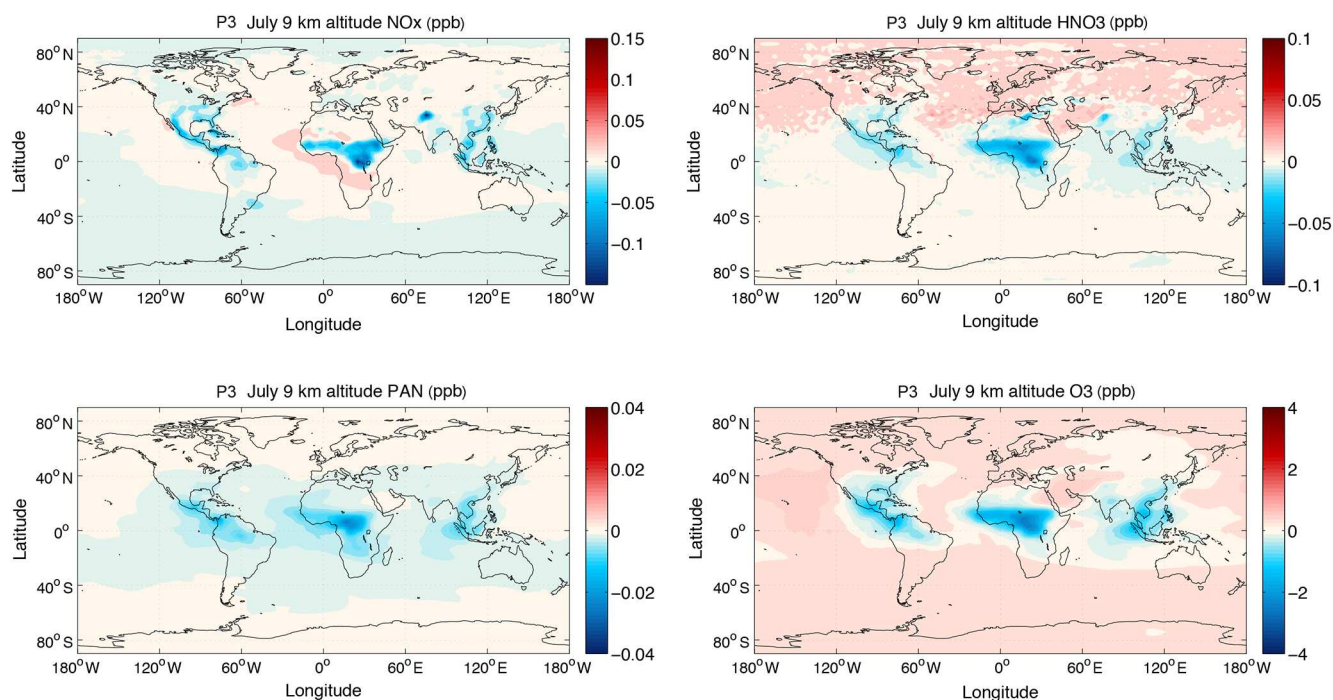


Figure 5. Geographical distributions of NO_x, HNO₃, PAN, and O₃ variations (in ppb) at 9 km altitude for July from the absolute difference (P3) between P1 and BC experiments. P1 was performed using τ and K_{eff} determined with $D_h = 15 \text{ m}^2 \text{ s}^{-1}$ and $\text{NO}_i^{\text{mean}}$ with GEOS-Chem.

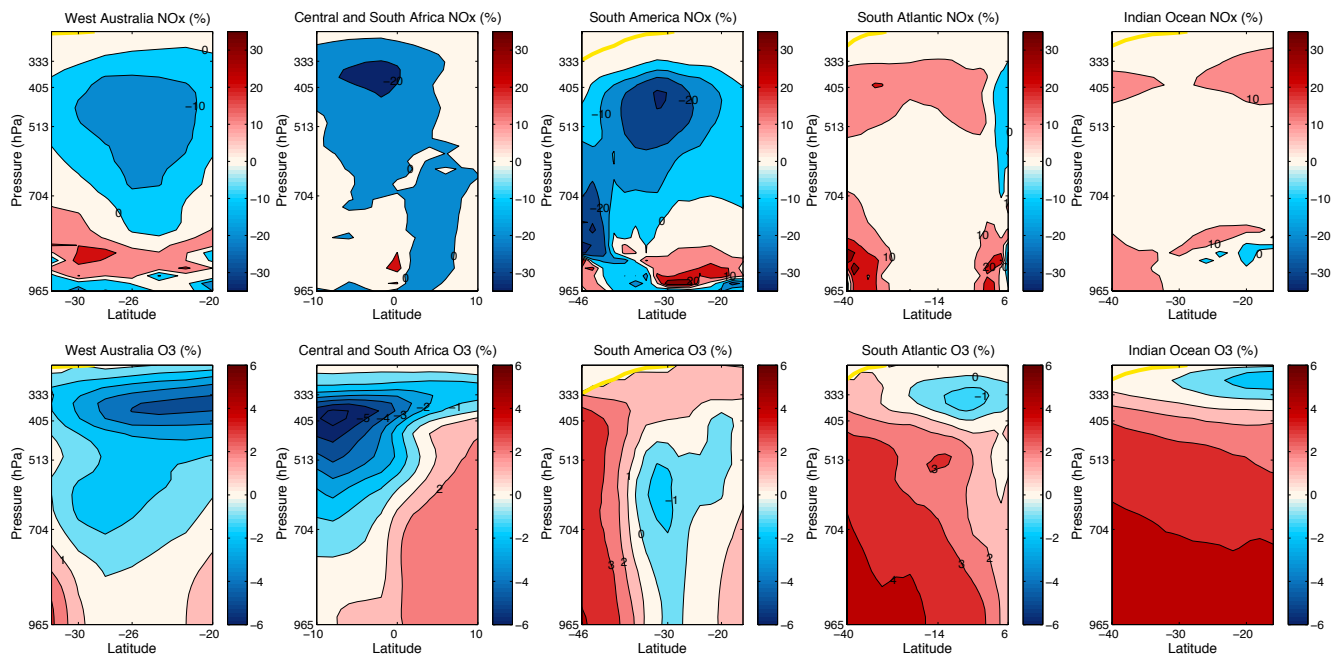


Figure 6. Zonal averaged NO_x (upper panels) and O₃ (bottom panels) variations (in %) over the regions characterized by strong NO_x emissions for January (the yellow solid line represents the tropopause level) from the relative difference between P1 and BC experiments (P3/BC). P1 was performed using τ and K_{eff} determined with $D_h = 15 \text{ m}^2 \text{ s}^{-1}$ and $\text{NO}_i^{\text{mean}}$ with GEOS-Chem.

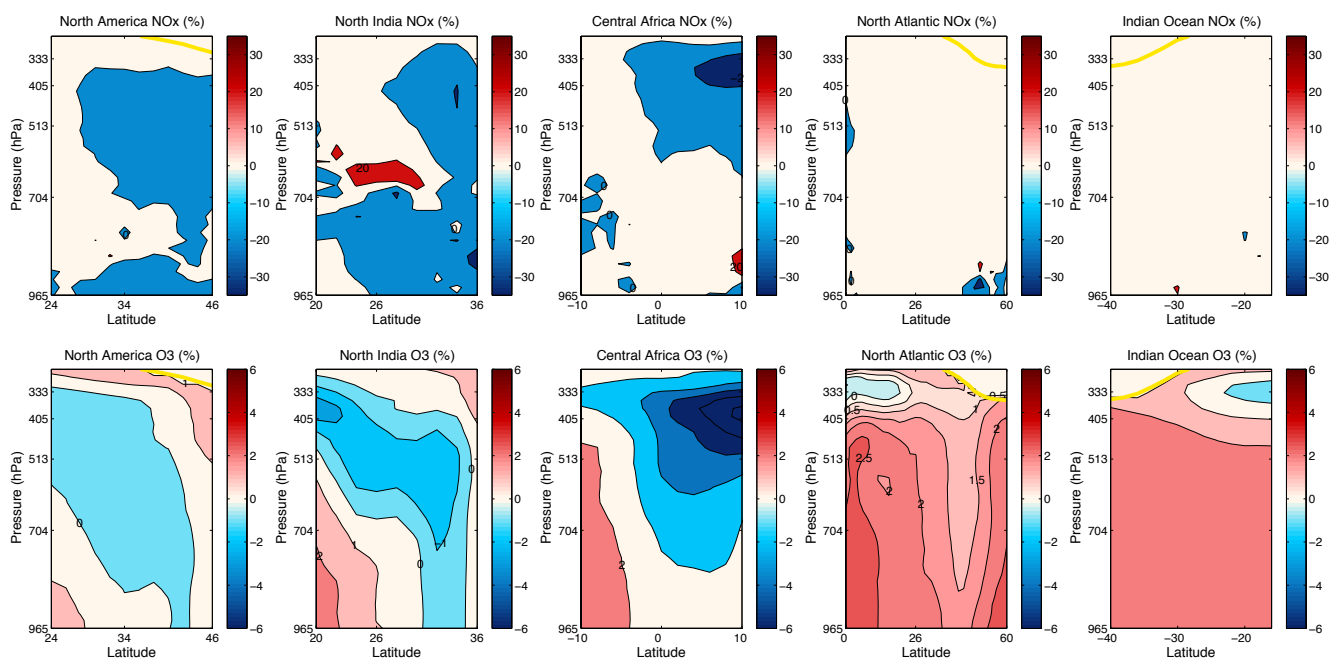


Figure 7. Zonal averaged NO_x (upper panels) and O₃ (bottom panels) variations (in %) over the regions characterized by strong NO_x emissions for July (the yellow solid line represents the tropopause level) from the relative difference between P1 and BC experiments (P3/BC). P1 was performed using τ and K_{eff} determined with $D_h = 15 \text{ m}^2 \text{ s}^{-1}$ and $\text{NO}_i^{\text{mean}}$ with GEOS-Chem.

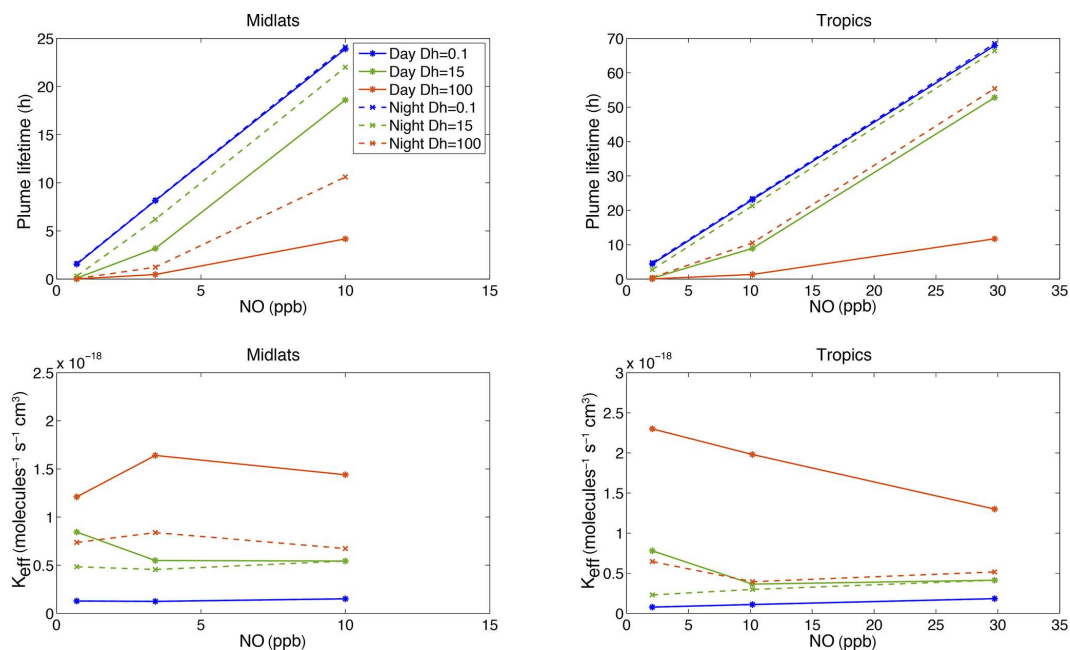


Figure 8. The plume lifetime (τ , upper panels) and the effective reaction rate constant (K_{eff} , bottom panels) depending (i) on the horizontal coefficient diffusion (D_h , m² s⁻¹) for the midlatitudes (left panels) and the tropics (right panels) and (ii) on the NO mixing ratio injected by lightning (NO_i , in ppb).

and ozone mixing ratios on a large scale over regions characterized by intense lightning emissions and (ii) an increase in these species downwind of emissions. In particular, the plume parameterization related to the lightning NO_x leads to

1. significant effects on the NO_x mixing ratio ($\pm 20\%$): these effects on nitrogen oxides are important because NO_x is the first criterion which is constrained in a CTM in order to determine the global LNO_x production (6 TgN yr⁻¹ in the GEOS-Chem model);
2. lower effects on the O₃ mixing ratio ($\pm 5\%$): these limited impacts on ozone may be explained by the compensatory effect of the NO_y species (mainly conversion of NO_x into HNO₃ within the plume).

The effects of the plume parameterization are simulated over the entire troposphere mainly for ozone. Indeed, the spreading of effects on ozone to the lower free troposphere is related to the subsidence areas of the Walker circulation. These regions are characterized by the accumulation and creation of ozone for low-altitude levels. Nevertheless, the maximum NO_x and O₃ variations are calculated for altitude levels associated with a mean detrainment level. The more realistic representation of the sub-grid processes (P1 experiment) related to the LNO_x plume is in contrast with the simplified instantaneous dilution in the grid cell of the lightning NO_x emissions (BC experiment).

The plume approach allows the conversion of NO_x into HNO₃ during the plume lifetime. In addition, the high NO_x

concentration within the plume (much higher than the background content) leads to the O₃ titration and more generally to the O_x destruction within the plume. The most important impact of the plume parameterization is the transport of the LNO_x emissions as a plume and the transport of the associated nonlinear chemistry effects, leading to a delay in the O₃ production on a large scale. In other words, less O₃ is produced by photochemical reactions from NO_x over the regions with intense lightning NO_x emissions than downwind of LNO_x emissions.

4.3 Plume sensitivity to the estimated uncertainties of parameter calculations

4.3.1 The atmospheric dynamical conditions and the initial NO mixing ratio injected by lightning

The impact of (i) the diffusion properties of the atmosphere (D_h) and (ii) the initial NO mixing ratio injected by lightning (NO_i) is analyzed. D_h and NO_i are the two key parameters in the determination of the physical and chemical characteristics of the plume. The modified simulation characterizing the P1 experiment was run for the ranges of the horizontal diffusion coefficients and the initial NO mixing ratio injected by lightning. It is important to note that for these sensitivity tests, the β_1 and β_2 coefficients remain constant in their mean values. The τ and K_{eff} values related to these simulations are those previously calculated (Sect. 3) and summarized in Tables 2 and 3. Figure 8 displays τ (upper panels) and K_{eff}

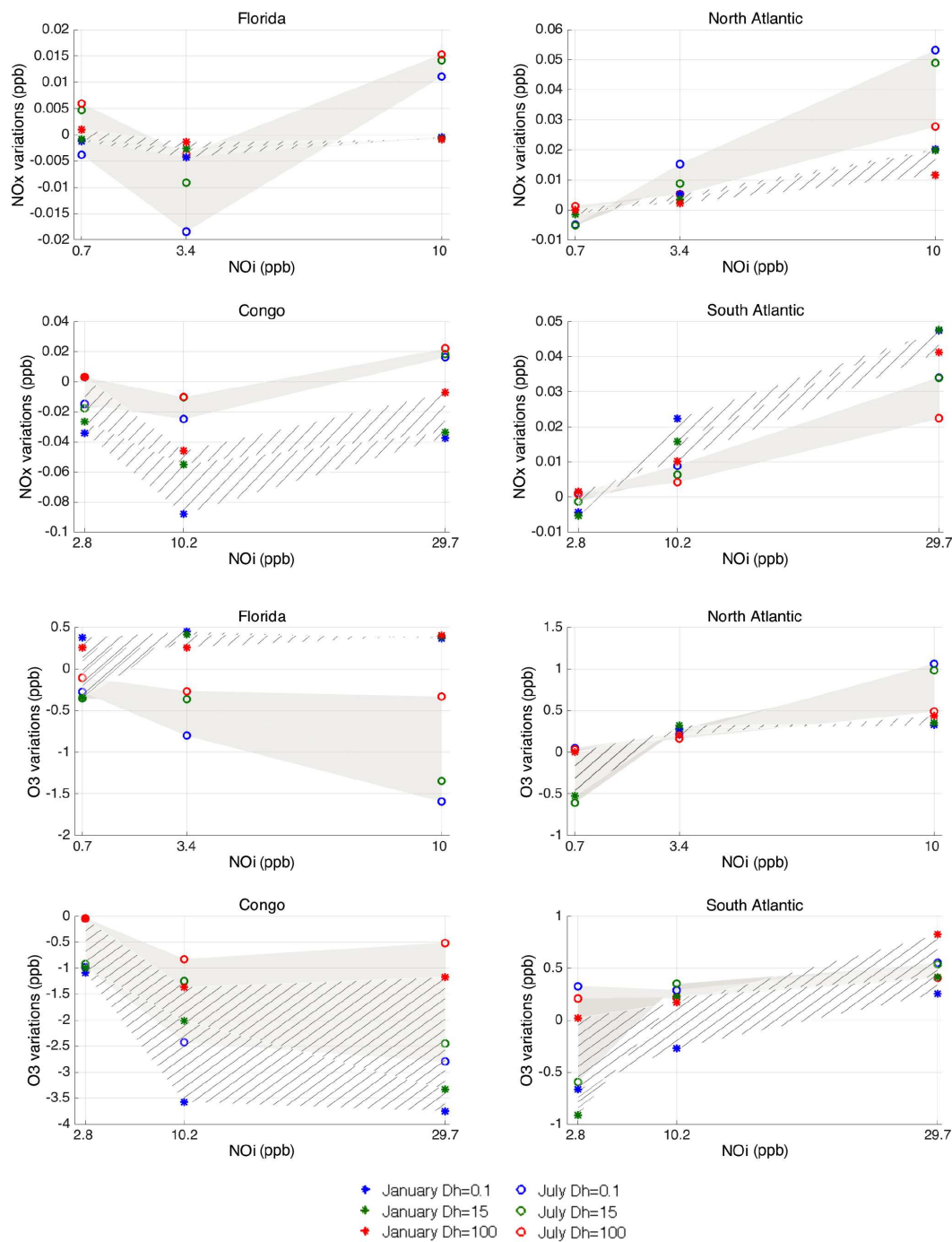


Figure 9. The NO_x and O₃ sensitivity at 9 km altitude depending on the horizontal coefficient diffusion (D_h , $\text{m}^2 \text{s}^{-1}$) and on the NO mixing ratio injected by lightning (NO_i , ppb) for the midlatitudes (Florida and North Atlantic) and the tropics (Congo Basin and South Atlantic). Intervals are hatched in January and filled in grey in July. Markers correspond to the NO_x variations simulated for $D_h = 0.1 \text{ m}^2 \text{ s}^{-1}$ (red), $D_h = 15 \text{ m}^2 \text{ s}^{-1}$ (blue), and $D_h = 100 \text{ m}^2 \text{ s}^{-1}$ (green).

Table 6. The sensitivity of NO_x (in ppt) and O₃ (in ppb) depending on the horizontal diffusion coefficient (D_h , m² s⁻¹) and on the NO_i mixing ratio (ppb) injected by lightning for the midlatitudes (Florida and North Atlantic) and tropics (Congo Basin and South Atlantic) in January and July.

| | Jan | | | | Jul | | | |
|-------------------------|----------------|----------------|----------------|----------------|----------------|----------------|----------------|----------------|
| | Midlatitudes | | Tropics | | Midlatitudes | | Tropics | |
| | Florida | North Atlantic | Congo Basin | South Atlantic | Florida | North Atlantic | Congo Basin | South Atlantic |
| $\Delta\text{NO}_x \pm$ | [-1.7, +1.8] | [-8.2, +1.7] | [-33.1 +29.7] | [-6.5, +6.9] | [-9.3, +5.4] | [-21.1, +6.6] | [-14.3, +21] | [-11.5, +2.6] |
| $\Delta\text{O}_3 \pm$ | [-0.16, +0.72] | [-0.12, +0.53] | [-1.56, +2.16] | [-0.49, +0.94] | [-0.44, +1.01] | [-0.49, +0.66] | [-1.18, +1.93] | [-0.14, +0.92] |

Table 7. The sensitivity of NO_x (in ppt) and O₃ (in ppb) depending on β_1 and β_2 values for the midlatitudes (Florida and North Atlantic) and tropics (Congo Basin and South Atlantic) in January and July. Experiment P1, using $D_h = 15 \text{ m}^2 \text{ s}^{-1}$ and NO_i^{mean}, performed with the GEOS-Chem model.

| | Jan | | | | Jul | | | |
|----------------------------------------|---------------|----------------|--------------|----------------|--------------|----------------|--------------|----------------|
| | Midlatitudes | | Tropics | | Midlatitudes | | Tropics | |
| | Florida | North Atlantic | Congo Basin | South Atlantic | Florida | North Atlantic | Congo Basin | South Atlantic |
| $\Delta\text{NO}_x \pm \times 10^{-2}$ | [-1.6, -0.06] | [-2.3, -2.3] | [-2.3, +0.9] | [+0.3, +0.6] | [-3.3, +1.4] | [-21.1, +6.6] | [+0.4, +2.1] | [-0.9, -0.4] |
| $\Delta\text{O}_3 \pm \times 10^{-4}$ | [-9, +5] | [-9, +4] | [-3, +22] | [-10, +11] | [-24, -6] | [-6, +19] | [-8, +17] | [-30, -2] |

(bottom panels) variations depending on D_h and NO_i. As expected, the strongest horizontal diffusion leads to the most efficient dispersion of the plume. In both the midlatitudes and the tropics, τ decreases when D_h becomes larger. In addition, τ increases with the initial NO mixing ratio injected by lightning. In contrast, K_{eff} increases with the D_h coefficient in the two regions of the globe.

The sensitivity of the NO_x and O₃ mixing ratios around the mean value for regions and seasons depending on the known uncertainties associated with parameter calculations has been quantified. Figure 9 shows the ranges of sensitivity of NO_x and O₃ (ΔNO_x and ΔO_3 , respectively) at 9 km altitude reproduced by GEOS-Chem depending on D_h and on the initial NO mixing ratio (NO_i). Note that for the sake of readability, the scale of NO_x and O₃ changes differs by region. Results are also summarized in Table 6.

We chose representative continental areas such as Florida and the Congo Basin, which correspond to regions characterized by intense electrical activity for the midlatitudes and the tropics, respectively. The North and South Atlantic were selected to represent regions downwind of NO_x emissions for the midlatitude and the tropics variations, respectively. The highest NO_x and O₃ ranges are obtained for continental tropical regions with ΔNO_x [-33.1, +29.7] ppt and ΔO_3 [-1.56, +2.16] ppb, in January, and ΔNO_x [-14.3, +21] ppt and ΔO_3 [-1.18, +1.93] ppb, in July. The largest range associated with the tropical continents may be explained by the largest difference in parameter values defining the plume in this region (especially NO_i). The smallest changes are observed over continental midlatitude regions for winter with ΔNO_x [-1.7, +1.8] ppt and ΔO_3 [-0.16, +0.72] ppb and over oceanic tropical regions in summer such that ΔNO_x [-11.5, +2.6] ppt and ΔO_3 [-0.14, +0.92] ppb. As a result, the sensitivity of NO_x and O₃ species to the pa-

rameter uncertainties is a few parts per trillion for NO_x and less than 2 ppb for O₃.

4.3.2 Coefficients related to the nitrification mechanism (β_1 and β_2)

In order to estimate the sensitivity of the NO_x and O₃ mixing ratios related to the uncertainties in the β_1 and β_2 fractions (Table 7), the difference between the P1 experiment using the β_1 and β_2 mean values and the P1 experiment using minimum and maximum β_1 and β_2 coefficients has been calculated. This implies that τ and K_{eff} are constant.

In January, the highest sensitivity in NO_x mixing ratio is ΔNO_x [-2.3, +0.9] $\times 10^{-2}$ ppt over the continental tropical regions and ΔO_3 [-10, +11] $\times 10^{-4}$ ppb over the tropical ocean in O₃, while the midlatitude oceanic areas show minimum ranges in NO_x and O₃, with $\Delta\text{NO}_x \pm 2.3 \times 10^{-2}$ ppt associated with ΔO_3 [-9, +4] $\times 10^{-4}$ ppb. In July, the maximum ranges are calculated over oceans in the midlatitudes for NO_x, such that ΔNO_x [-21.1, +6.6] $\times 10^{-2}$ ppt, and in the tropics for O₃, with ΔO_3 [-30, -2] $\times 10^{-4}$ ppb. Finally, the smallest changes, ΔNO_x [-0.9, -0.4] $\times 10^{-2}$ ppt and ΔO_3 [-24, -6] $\times 10^{-4}$ ppb, are simulated for the tropical ocean and the midlatitude continents, respectively.

In addition, the impact of the nitrification mechanism was assessed comparing the P1 experiment using mean β_1 and β_2 values and the P2 experiment for which $\beta_1 = \beta_2 = 0$. As a result, taking into account NO_x conversion into HNO₃ and using the mean β fractions calculated in this study does not imply strong changes in NO_x and O₃ distributions ($\Delta\text{NO}_x < 10^{-4}$ ppt and $\Delta\text{O}_3 < 10^{-2}$ ppb).

In the case of significant values of the β fractions, the rate of the nitrification mechanism should imply a delay in the O₃ formation from the NO_x in the plume because of the NO_x storage in HNO₃. On the other hand, HNO₃ is considered one

of the main sinks for NO_x species undergoing wet deposition and seemingly limiting their affect on global ozone.

The sensitivity tests indicate the limited effect of the NO_x conversion to HNO₃ within the plume using our β_1 and β_2 calculations. The sensitivity on NO_x and O₃ mixing ratios related to β coefficients is about a few parts per trillion. Indeed, our β_1 and β_2 estimates are smaller than those calculated by Cariolle et al. (2009) ($\beta_1 = 0.06$ and $\beta_2 = 0.2$), which showed a large impact of this mechanism in the case of aircraft NO_x emissions. In the present study, we can easily suppose that the increase in the β_1 and β_2 coefficients should be in agreement with the work of Cooper et al. (2014) in reducing the underestimate of the HNO₃ production induced by NO_x emissions from lightning. Further estimates of β should be realized using future observations in the cloud anvil of primary species, aerosols, and particles needed for NO_x conversion during the daytime and nighttime to improve the determination of these parameters. The β_1 coefficient is particularly dependent on the HO_x radicals, which may vary significantly within the cloud anvil, in part because of the transport of peroxides from the lower troposphere by convective uplift (Wennberg et al., 1998). The determination of β_2 , corresponding to the NO_x conversion fraction into HNO₃ via N₂O₅ formation during nighttime is considerably dependent on (i) the estimate of aerosols and the ice crystal concentration and their lifetime within the cloud anvil, which is highly uncertain according to measurement campaigns, and (ii) the reaction probability regarding aerosols $\gamma_{\text{N}_2\text{O}_5}^{\text{aerosol}}$ and ice crystals $\gamma_{\text{N}_2\text{O}_5}^{\text{ice}}$ from laboratory study extrapolations.

According to the results presented in this section, the sensitivity tests show the predominance of the initial NO mixing ratio injected by lightning (NO_i) and the diffusion properties of the atmosphere (D_h) in the variability of the NO_x and O₃ mixing ratios around the mean value in response to the plume-in-grid parameterization in the CTM. In winter, the NO_x and O₃ sensitivity is the highest for continental regions in the tropics and the smallest sensitivity is calculated for the midlatitudes. In summer, the most important sensitivity of NO_x and O₃ is simulated in the tropics over regions characterized by intense LNO_x emissions, while the least significant sensitivity is still obtained in the tropics but downwind of emissions (mainly over oceans).

5 Conclusions

For the first time, a more realistic lightning NO_x chemistry is implemented as a plume parameterization in a global chemical transport model. The key parameters characterizing the lightning-related plume were estimated depending on two main criteria, i.e., the NO mixing ratio injected by lightning (NO_i) and the atmospheric diffusion coefficient (D_h).

According to the NO_i and D_h ranges, the plume lifetime (τ) and the effective reaction rate constant (K_{eff}) for NO_x-O₃ chemical interactions were estimated as follows:

$$- \tau = [0.01, 68.5] \text{ h};$$

$$- K_{\text{eff}} = [0.77, 23] \times 10^{-19} \text{ molecules}^{-1} \text{ s}^{-1} \text{ cm}^3.$$

Also, for the conditions defined by NO_i^{mean} and $D_h = 15 \text{ m}^2 \text{ s}^{-1}$

$$- \tau \text{ is } 3 \text{ (6) h in the midlatitudes and } 9 \text{ (21.3) h in the tropics during the daytime (nighttime);}$$

$$- K_{\text{eff}} \text{ is } 5.49 \times 10^{-19} \text{ molecules}^{-1} \text{ s}^{-1} \text{ cm}^3 \text{ (} 4.55 \times 10^{-19} \text{ molecules}^{-1} \text{ s}^{-1} \text{ cm}^3 \text{) in the midlatitudes and } 3.64 \times 10^{-19} \text{ molecules}^{-1} \text{ s}^{-1} \text{ cm}^3 \text{ (} 2.98 \times 10^{-19} \text{ molecules}^{-1} \text{ s}^{-1} \text{ cm}^3 \text{) in the tropics during the daytime (nighttime).}$$

Finally, the fractions of NO_x conversion into HNO₃ within the plume are $\beta_1 = [1.34, 1.88] \times 10^{-4}$ and $\beta_2 = [0.24, 14.4] \times 10^{-3}$ for day and night conditions, respectively.

GEOS-Chem simulations performed using mean values for NO_i and $D_h = 15 \text{ m}^2 \text{ s}^{-1}$ reveal nitrogen species and ozone changes compared to the instantaneous dilution. A decrease in NO_x and O₃ mixing ratios on a large scale over regions of strong LNO_x emissions is observed mainly in the Northern Hemisphere in summer and in the Southern Hemisphere in winter. In the troposphere, a maximum decrease of 20 % (6 %) in January and 25 % (8 %) in July for NO_x (O₃) is found over central Africa. In contrast, an increase in NO_x (O₃) downwind of emissions of 20 % (4 %) in January and 18 % (2 %) in July is simulated. The LNO_x plume parameterization allows the transport of the effects on the nonlinear chemistry occurring within the plume and the conversion of NO_x to nitrogen reservoir species (mainly HNO₃). However, the most significant impact is the transport of the LNO_x as a plume. This implies a delay of (i) the NO_x release into the point grid and (ii) ozone production from NO_x emitted by lightning flashes corresponding to the decrease in the NO_x and O₃ mixing ratios on a large scale over regions of emissions and their increase over the transport pathway.

The sensitivity of the NO_x and O₃ mixing ratios around the mean value depending on the known uncertainties in the plume physics and chemistry key parameters has been estimated. The highest sensitivity is obtained for the continental tropical regions with $\Delta\text{NO}_x [-33.1, +29.7] \text{ ppt}$ and $\Delta\text{O}_3 [-1.56, +2.16] \text{ ppb}$, in January, and $\Delta\text{NO}_x [-14.3, +21] \text{ ppt}$ and $\Delta\text{O}_3 [-1.18, +1.93] \text{ ppb}$, in July. Concerning the β_1 and β_2 fractions, the highest sensitivity depending on the fraction uncertainties for NO_x is $\Delta\text{NO}_x [-2.3, +0.9] \times 10^{-2} \text{ ppt}$ over the continental tropical regions and $\Delta\text{O}_3 [-10, +11] \times 10^{-4} \text{ ppb}$ for O₃ over the tropical ocean in January. In summer, the maximum ranges are calculated over oceans in the midlatitudes for NO_x, such as $\Delta\text{NO}_x [-21.1, +6.6] \times 10^{-2} \text{ ppt}$, and in the tropics for O₃, with $\Delta\text{O}_3 [-30, -2] \times 10^{-4} \text{ ppb}$. Accordingly, the parameters leading to the highest uncertainties in results and those which drive the plume-in-grid parameterization are NO_i and D_h .

This study demonstrates the importance of considering the plume-in-grid chemistry related to the lightning NO_x emissions occurring on a smaller scale for global calculations. Taking into account the plume dilution into the background atmosphere in time and space with the transport of the NO_x and O₃ nonlinear chemistry effects and the conversion of NO_x into HNO₃ reservoir species implies more realistic NO_x and O₃ concentrations in CTM. By allowing a more realistic sub-grid chemistry, the plume-in-grid approach will allow the improvement of the different steps in lightning NO_x emissions modeling, such as the convection process, the calculation of the NO molecules produced by lightning discharges depending on regions according to recent and future satellite observations, and also processes such as HNO₃ scavenging and HNO₃ uptake by ice crystals.

Acknowledgements. The GEOS-Chem community (Harvard University) and the Laboratoire d'Aérodynamique (UPS/CNRS) supported this work. The authors acknowledge the help of Lee T. Murray (NASA, NY, USA) and his expertise on the lightning NO_x emissions module in the GEOS-Chem model. We thank the University Paul Sabatier III of Toulouse for the ATUPS grant, which allowed collaboration with the Wolfson Atmospheric Chemistry Laboratories of York and the research group of Mathew J. Evans.

Edited by: C. H. Song

References

- Amos, H. M., Jacob, D. J., Holmes, C. D., Fisher, J. A., Wang, Q., Yantosca, R. M., Corbett, E. S., Galarneau, E., Rutter, A. P., Gustin, M. S., Steffen, A., Schauer, J. J., Graydon, J. A., Louis, V. L. St., Talbot, R. W., Edgerton, E. S., Zhang, Y., and Sunderland, E. M.: Gas-particle partitioning of atmospheric Hg(II) and its effect on global mercury deposition, *Atmos. Chem. Phys.*, 12, 591–603, doi:10.5194/acp-12-591-2012, 2012.
- Aumont, B.: Modélisation de la chimie troposphérique, Manuscript presented for the degree of “Habilitation à diriger les recherches”, Université Paris 12, Val de Marne, UFR de Sciences et Technologie, 2005.
- Banerjee, A., Archibald, A. T., Maycock, A. C., Telford, P., Abraham, N. L., Yang, X., Braesicke, P., and Pyle, J. A.: Lightning NO_x, a key chemistry-climate interaction: impacts of future climate change and consequences for tropospheric oxidising capacity, *Atmos. Chem. Phys.*, 14, 9871–9881, doi:10.5194/acp-14-9871-2014, 2014.
- Bechtold, P., Bazile, E., Guichard, F., Mascart, P., and Richard, E.: A mass-flux convection scheme for regional and global models, *Q. J. Roy. Meteor. Soc.*, 127, 869–886, 2000.
- Bey, I., Jacob, D. J., Yantosca, R. M., Logan, J. A., Field, B. D., Fiore, A. M., Li, Q., Liu, H. Y., Mickley, L. J., and Schultz, M. G.: Global modeling of tropospheric chemistry with assimilated meteorology: model description and evaluation, *J. Geophys. Res.*, 106, 23073–23095, 2001.
- Bian, H. and Prather, M. J.: Fast-J2: Accurate simulation of stratospheric photolysis in global chemical models, *J. Atmos. Chem.*, 41, 281–296, 2002.
- Cariolle, D., Caro, D., Paoli, R., Hauglustaine, D. A., Cuénot, B., Cozic, A., and Paugam, R.: Parametrization of plume chemistry into large-scale atmospheric models: application to aircraft NO_x emissions, *J. Geophys. Res.*, 114, D19302, doi:10.1029/2009JD011873, 2009.
- Choi, Y., Kim, J., Eldering, A., Osterman, G., Yung, Y. L., Gu, Y., and Liou, K. N.: Lightning and anthropogenic NO_x sources over the United States and the western North Atlantic Ocean: impact on OLR and radiative effects, *Geophys. Res. Lett.*, 36, L17806, doi:10.1029/2009GL039381, 2009.
- Christian, H. J., Blakeslee, R. J., Boccippio, D. J., Boeck, W. L., Buechler, D. E., Driscoll, K. T., Goodman, S. J., Hall, J. M., Koshak, W. J., Mach, D. M., and Stewart, M. F.: Global frequency and distribution of lightning as observed from space by the Optical Transient Detector, *J. Geophys. Res.*, 108, 4005, doi:10.1029/2002JD002347, 2003.
- Cohard, J.-M. and Pinty, J. P.: A comprehensive two-moment warm microphysical bulk scheme. I: Description and tests, *Q. J. Roy. Meteor. Soc.*, 126, 1815–1842, 2000.
- Cooper, M., Martin, R. V., Wespes, C., Coheur, P.-F., Clerbaux, C., and Murray L. T.: Tropospheric nitric acid columns from the IASI satellite instrument interpreted with a chemical transport model: implications for parameterizations of nitric oxide production by lightning, *J. Geophys. Res.*, 119, 10068–10079, 2014.
- Cuxart, J., Bougeault, P., and Redelsperger, J. L.: A turbulence scheme allowing for mesoscale and large-eddy simulations, *Q. J. Roy. Meteor. Soc.*, 126, 1–30, 1999.
- Damian, V., Sandu, A., Damian, M., Potra, F., and Camichael, G. R.: The kinetic preprocessor KPP – a software environment for solving chemical kinetics, *Comput. Chem. Eng.*, 26, 1567–1579, 2002.
- Dye, J. E., Ridley, B. A., Skamarock, W., Barth, M., and Venticini, M.: An overview of the Stratospheric-Tropospheric experiment: radiation, aerosols, and ozone (STERAO)-Deep convection experiment with results for the July 10, 1996 storm, *J. Geophys. Res.*, 105, 10023–10045, 2000.
- Emmerson, K. M. and Evans, M. J.: Comparison of tropospheric gas-phase chemistry schemes for use within global models, *Atmos. Chem. Phys.*, 9, 1831–1845, doi:10.5194/acp-9-1831-2009, 2009.
- Evans, M. J. and Jacob, D. J.: Impact of new laboratory studies of N₂O₅ hydrolysis on global model budgets of tropospheric nitrogen oxides, ozone, and OH, *Geophys. Res. Lett.*, 32, L09813, doi:10.1029/2005GL022469, 2005.
- Franzblau, E.: Electrical discharges involving the formation of NO, NO₂, HNO₃ and O₃, *J. Geophys. Res.*, 96, 22337–22345, 1991.
- Gregory, D., Morcrette J.-J., Jakob, C., Beljaars, A. C. M., and Stockdale, T.: Revision of convection, radiation and cloud schemes in the ECMWF Integrated Forecasting System, *Q. J. Roy. Meteor. Soc.*, 126, 1685–1710, 2000.
- Grewe, V.: Impact of climate variability on tropospheric ozone, *Sci. Total Environ.*, 374, 167–181, 2007.
- Guenther, A. B., Jiang, X., Heald, C. L., Sakulyanontvittaya, T., Duhl, T., Emmons, L. K., and Wang, X.: The Model of Emissions of Gases and Aerosols from Nature version 2.1 (MEGAN2.1): an extended and updated framework for modeling biogenic emis-

- sions, *Geosci. Model Dev.*, 5, 1471–1492, doi:10.5194/gmd-5-1471-2012, 2012.
- Hauglustaine, D. A., Granier, C., and Brasseur, G. P.: Impact of present aircraft emissions of nitrogen oxides on tropospheric ozone and climate forcing, *Geophys. Res. Lett.*, 21, 2031–2034, 1994.
- Hauglustaine, D., Emmons, L., Newchurch, M., Brasseur, G., Takao, T., Matsubara, K., Johnson, J., Ridley, B., Stith, J., and Dye, J.: On the role of lightning NO_x in the formation of tropospheric ozone plumes: a global model perspective, *J. Atmos. Chem.*, 38, 277–294, 2001.
- Hudman, R. C., Jacob, D. J., Turquety, S., Leibensperger, E. M., Murray, L. T., Wu, S., Gilliland, A. B., Avery, M., Bertram, T. H., Brune, W., Cohen, R. C., Dibb, J. E., Flocke, F. M., Fried, A., Holloway, J., Neuman, J. A., Orville, R., Perring, A., Ren, X., Sachse, G. W., Singh, H. B., Swanson, A., and Wooldridge, P. J.: Surface and lightning sources of nitrogen oxides over the United States: Magnitudes, chemical evolution, and outflow, *J. Geophys. Res.*, 112, D12S05, doi:10.1029/2006JD007912, 2007.
- Huntrieser, H., Schlager, H., Feigl, C., and Höller, H.: Transport and production of NO_x in electrified thunderstorms: survey of previous studies and new observations at midlatitudes, *J. Geophys. Res.*, 103, 28247–28264, 1998.
- Huntrieser, H., Feigl, C., Schlager, H., Schröder, F., Gerbig, C., and van Velthoven, P.: Airborne measurements of NO_x, tracer species, and small particles during the European Lightning Nitrogen Oxides Experiment, *J. Geophys. Res.*, 107, 4113, doi:10.1029/2000JD000209, 2002.
- Huszar, P., Cariolle, D., Paoli, R., Halenka, T., Belda, M., Schlager, H., Miksovsky, J., and Pisoft, P.: Modeling the regional impact of ship emissions on NO_x and ozone levels over the Eastern Atlantic and Western Europe using ship plume parameterization, *Atmos. Chem. Phys.*, 10, 6645–6660, doi:10.5194/acp-10-6645-2010, 2010.
- Jacobson, M. Z. and Turco, R. P.: SMVGear: a sparse-matrix, vectorized gear code for atmospheric models, *Atmos. Environ.*, 28, 273–284, 1994.
- Jaéglé, L., Jacob, D. J., Wang, Y., Weinheimer, A. J., Ridley, B. A., Campos, T. L., Sachse, G. W., and Hagen, D. E.: Sources and chemistry of NO_x in the upper troposphere over the United States, *Geophys. Res. Lett.*, 25, 1705–1708, 1998.
- Jenkin, M. E., Saunders, S. M., and Pilling, M. J.: The tropospheric degradation of volatile organic compounds: a protocol for mechanism development, *Atmos. Environ.*, 31, 81–104, 1997.
- Klemp, J. B. and Wilhelmson, R. B.: The simulation of three-dimensional convective storm dynamics, *J. Atmos. Sci.*, 35, 1070–1096, 1978.
- Knollenberg, R. G.: Measurements of the growth of the ice budget in a persisting contrail, *J. Atmos. Sci.*, 29, 1367–1374, 1972.
- Knollenberg, R. G., Kelly, K., and Wilson, J. C.: Measurements of high number densities of ice crystals in the tops of tropical cumulonimbus, *J. Geophys. Res.*, 98, 8639–8664, 1993.
- Labrador, L. J., von Kuhlmann, R., and Lawrence, M. G.: Strong sensitivity of the global mean OH concentration and the tropospheric oxidizing efficiency to the source of NO_x from lightning, *Geophys. Res. Lett.*, 31, L06102, doi:10.1029/2003GL019229, 2004.
- Lafore, J. P., Stein, J., Asencio, N., Bougeault, P., Ducrocq, V., Duron, J., Fischer, C., Hérelil, P., Mascart, P., Masson, V., Pinty, J. P., Redelsperger, J. L., Richard, E., and Vilà-Guerau de Arellano, J.: The Meso-NH Atmospheric Simulation System. Part I: adiabatic formulation and control simulations, *Ann. Geophys.*, 16, 90–109, doi:10.1007/s00585-997-0090-6, 1998.
- Lange, L., Hoor, P., Helas, G., Fischer, H., Brunner, D., Scheeren, B., Williams, J., Wong, S., Wohlfrom, K.-H., Arnold, F., Strom, J., Krejci, R., Lelieveld, J., and Andreae, M. O.: Detection of lightning-produced NO in the midlatitude upper troposphere during STREAM 1998, *J. Geophys. Res.*, 106, 27777–27785, 2001.
- Lascaux, F., Richard, E., and Pinty, J. P.: Numerical simulations of three different MAP IOPs and the associated microphysical processes, *Q. J. Roy. Meteor. Soc.*, 132, 1907–1926, 2006.
- Lin, J.-T. and McElroy, M. B.: Impacts of boundary layer mixing on pollutant vertical profiles in the lower troposphere: implications to satellite remote sensing, *Atmos. Environ.*, 44, 1726–1739, 2010.
- Lin, S.-J. and Rood, R. B.: Multidimensional flux-form semi-lagrangian transport scheme, *Mon. Weather Rev.*, 124, 2046–2070, 1996.
- Lin, X., Trainer, M., and Liu, S. C.: On the nonlinearity of the tropospheric ozone production, *J. Geophys. Res.*, 93, 15879–15888, 1988.
- Liu, H., Jacob, D. J., Rey, I., and Yantosca, R. M.: Constraints from ²¹⁰Pb and ⁷Be on wet deposition and transport in a global three-dimensional chemical tracer model driven by assimilated meteorological fields, *J. Geophys. Res.*, 106, 12109–12128, 2001.
- Madronich, S. and Flocke, S.: *Environmental Photochemistry*, doi:10.1007/978-3-540-69044-3, Springer Berlin Heidelberg, 1999.
- Martin, R. V., Jacob, D. J., Logan, J. A., Bey, I., Yantosca, R. M., Staudt, A. C., Li, Q., Fiore, A. M., Duncan, B. N., and Liu, H.: Interpretation of TOMS observations of tropical tropospheric ozone with a global model and in situ observations, *J. Geophys. Res.*, 107, 4351, doi:10.1029/2001JD001480, 2002.
- Martin, R. V., Jacob, D. J., Yantosca, R. M., Chin, M., and Ginoux, P.: Global and Regional Decreases in Tropospheric Oxidants from Photochemical Effects of Aerosols, *J. Geophys. Res.*, 108, 4097, doi:10.1029/2002jd002622, 2003.
- Martin, R. V., Sauvage, B., Folkins, I., Sioris, C. E., Boone, C., Bernath, P., and Ziemke, J.: Space-based constraints on the production of nitric oxide by lightning, *J. Geophys. Res.*, 112, D09309, doi:10.1029/2006JD007831, 2007.
- Monks, P. S.: Gas-phase radical chemistry in the troposphere, *Chem. Soc. Rev.*, 34, 376–395, 2005.
- Moorthi, S. and Suarez, M. J.: Relaxed Arakawa-Schubert: a parameterization of moist convection for general circulation models, *Mon. Weather Rev.*, 120, 978–1002, 1991.
- Murray, L. T., Jacob, D. J., Logan, J. A., Hudman, R. C., and Koshak, J.: Optimized regional and interannual variability of lightning in a global chemical transport model constrained by LIS/OTD satellite data, *J. Geophys. Res.*, 117, D20307, doi:10.1029/2012JD017934, 2012.
- Olivier, J. G. J.: Recent trends in global greenhouse gas emissions: regional trends and spatial distribution of key sources, *Environ. Sci.*, 2, 81–89, 2005.
- Ott, L. E., Pickering, K. E., Stenichkov, G. L., Allen, D. J., DeCaria, A. J., Ridley, B., Lin, R.-F., Lang, S., and Tao, W.-K.: Production of lightning NO_x and its vertical distribution calculated from three-dimensional cloud-scale chemical

- transport model simulations, *J. Geophys. Res.*, 115, D04301, doi:10.1029/2009JD011880, 2010.
- Paoli, R., Cariolle, D., and Sausen, R.: Review of effective emissions modeling and computation, *Geosci. Model Dev.*, 4, 643–667, doi:10.5194/gmd-4-643-2011, 2011.
- Pickering, K. E., Thompson, A. M., Dickerson, R. R., Luke, W. T., MacNamara, D. P., Greenberg, J. P., and Zimmerman, P. R.: Model calculations of tropospheric ozone production potential following observed convective events, *J. Geophys. Res.*, 95, 14049–14062, 1990.
- Pinty, J. P. and Jabouille, P.: A mixed-phase cloud parameterization for use in a mesoscale non-hydrostatic model: simulations of a squall line and of orographic precipitation, in: Proceedings of Conference on Cloud Physics, 17–21 August 1998, Everett, USA, 217–220, 1998.
- Price, C. and Rind, D.: A simple lightning parameterization for calculating global lightning distributions, *J. Geophys. Res.*, 97, 9919–9933, 1992.
- Price, C. and Rind, D.: Possible implications of global climate change on global lightning distributions and frequencies, *J. Geophys. Res.*, 99, 10823–10831, 1994.
- Sander, S. P., Friedl, R. R., Golden, D. M., Kurylo, M. J., Moortgat, G. K., Wine, P. H., Ravishankara, A. R., Kolb, C. E., Molina, M. J., Finlayson-Pitts, B. J., Huie, R. E., and Orkin, V. L.: Chemical kinetics and photochemical data for use in atmospheric studies, evaluation number 15, Tech. rep., NASA, 2006.
- Saunders, S. M., Jenkin, M. E., Derwent, R. G., and Pilling, M. J.: Protocol for the development of the Master Chemical Mechanism, MCM v3 (Part A): tropospheric degradation of non-aromatic volatile organic compounds, *Atmos. Chem. Phys.*, 3, 161–180, doi:10.5194/acp-3-161-2003, 2003.
- Sauvage, B., Martin, R. V., van Donkelaar, A., and Ziemke, J. R.: Quantification of the factors controlling tropical tropospheric ozone and the South Atlantic maximum, *J. Geophys. Res.*, 112, D11309, doi:10.1029/2006JD008008, 2007a.
- Sauvage, B., Martin, R. V., van Donkelaar, A., Liu, X., Chance, K., Jaeglé, L., Palmer, P. I., Wu, S., and Fu, T.-M.: Remote sensed and in situ constraints on processes affecting tropical tropospheric ozone, *Atmos. Chem. Phys.*, 7, 815–838, doi:10.5194/acp-7-815-2007, 2007b.
- Schumann, U. and Huntrieser, H.: The global lightning-induced nitrogen oxides source, *Atmos. Chem. Phys.*, 7, 3823–3907, doi:10.5194/acp-7-3823-2007, 2007.
- Stark, M. S., Harrison, J. T. H., and Anastasi, C.: Formation of nitrogen oxides by electrical discharges and implications for atmospheric lightning, *J. Geophys. Res.*, 101, 6963–6969, 1996.
- Stith, J., Dye, J., Ridley, B., Laroche, P., Defer, E., Hübler, G., Zerr, R., and Venticinque, M.: NO signatures from lightning flashes, *J. Geophys. Res.*, 104, 16081–16089, 1999.
- Stockwell, D. Z., Giannakopoulos, C., Plantevin, P. H., Carver, G. D., Chipperfield, M. P., Law, K. S., Pyle, J. A., Shallcross, D. E., and Wang, K. Y.: Modelling NO_x from lightning and its impact on global chemical fields, *Atmos. Environ.*, 33, 4477–4493, 1999.
- Streets, D. G., Zhang, Q., Wang, L., He, L., Hao, J., Wu, Y., Tang, Y., and Carmichael, G. R.: Revisiting China's CO emissions after the Transport and Chemical evolution over the Pacific (TRACE-P) mission: Synthesis of inventories, atmospheric modeling, and observations, *J. Geophys. Res.*, 111, D14306, doi:10.1029/2006JD007118, 2006.
- Teyssède, H., Michou, M., Clark, H. L., Josse, B., Karcher, F., Olivie, D., Peuch, V.-H., Saint-Martin, D., Cariolle, D., Attié, J.-L., Nédélec, P., Ricaud, P., Thouret, V., van der A, R. J., Volz-Thomas, A., and Chéroux, F.: A new tropospheric and stratospheric Chemistry and Transport Model MOCAGE-Climat for multi-year studies: evaluation of the present-day climatology and sensitivity to surface processes, *Atmos. Chem. Phys.*, 7, 5815–5860, doi:10.5194/acp-7-5815-2007, 2007.
- Tost, H., Jöckel, P., and Lelieveld, J.: Lightning and convection parameterisations – uncertainties in global modelling, *Atmos. Chem. Phys.*, 7, 4553–4568, doi:10.5194/acp-7-4553-2007, 2007.
- Trier, S. B. and Sharman, R. D.: Convection-permitting simulations of the environment supporting widespread turbulence within the upper-level outflow of a mesoscale convective system, *American Meteorological Society*, 137, 1972–1990, 2008.
- Tulet, P., Crassier, V., Solmon, F., Guedalia, D., and Rosset, R.: Description of the Mesoscale Nonhydrostatic chemistry model and application to a transboundary pollution episode between northern France and southern England, *J. Geophys. Res.*, 108, 4021, doi:10.1029/2000JD000301, 2003.
- Tulet, P., Grini, A., Griffin, R. J., and Petitcol, S.: ORILAM-SOA: A computationally efficient model for predicting secondary organic aerosols in three-dimensional atmospheric models, *J. Geophys. Res.*, 111, D23208, doi:10.1029/2006JD007152, 2006.
- van der Werf, G. R., Randerson, J. T., Giglio, L., Collatz, G. J., Mu, M., Kasibhatla, P. S., Morton, D. C., DeFries, R. S., Jin, Y., and van Leeuwen, T. T.: Global fire emissions and the contribution of deforestation, savanna, forest, agricultural, and peat fires (1997–2009), *Atmos. Chem. Phys.*, 10, 11707–11735, doi:10.5194/acp-10-11707-2010, 2010.
- Wang, Q., Jacob, D. J., Fisher, J. A., Mao, J., Leibensperger, E. M., Carouge, C. C., Le Sager, P., Kondo, Y., Jimenez, J. L., Cubison, M. J., and Doherty, S. J.: Sources of carbonaceous aerosols and deposited black carbon in the Arctic in winter-spring: implications for radiative forcing, *Atmos. Chem. Phys.*, 11, 12453–12473, doi:10.5194/acp-11-12453-2011, 2011.
- Wang, Y., Jacob, D. J., and Logan, J. A.: Global simulation of tropospheric O₃-NO_x-hydrocarbon chemistry – 1. Model formulation, *J. Geophys. Res.*, 103, 10713–10725, 1998.
- Wennberg, P. O., Hanisco, T. F., Jaegle, L., Jacob, D. J., Hints, E. J., Lanzendorf, E. J., Anderson, J. G., Gao, R.-S., Keim, E. J., Donnelly, S. G., Del Negro, L. A., Fahey, D. W., McKeen, S. A., Salawitch, R. J., Webster, C. R., May, R. D., Herman, R. L., Proffitt, M. H., Margitan, J. J., Atlas, E. L., Schauffler, S. M., Flocke, F., McElroy, C. T., and Bui, T. P.: Hydrogen radicals, nitrogen radicals and the production of O₃ in the upper troposphere, *Science*, 279, 49–53, doi:10.1126/science.279.5347.49, 1998.
- Wesely, M. L.: Parameterization of surface resistances to gaseous dry deposition in regional-scale numerical models, *Atmos. Environ.*, 23, 1293–1304, 1989.
- World Meteorological Organization (WMO): Scientific Assessment of Ozone Depletion: 1998, Tech. rep., World Meteorological Organization, Geneva, Switzerland, 1999.
- Yevich, R. and Logan, J. A.: An assessment of biofuel use and burning of agricultural waste in the developing world, *Global Biogeochem. Cy.*, 17, 1095, doi:10.1029/2002GB001952, 2003.

- Yienger, J. J. and Levy, H.: Empirical model of global soil-biogenic NO_x emissions, *J. Geophys. Res.*, 100, 11447–11464, 1995.
- Zhang, Q., Streets, D. G., Carmichael, G. R., He, K. B., Huo, H., Kannari, A., Klimont, Z., Park, I. S., Reddy, S., Fu, J. S., Chen, D., Duan, L., Lei, Y., Wang, L. T., and Yao, Z. L.: Asian emissions in 2006 for the NASA INTEX-B mission, *Atmos. Chem. Phys.*, 9, 5131–5153, doi:10.5194/acp-9-5131-2009, 2009.
- Zhang, R., Tie, X., and Bond, D. W.: Impacts of anthropogenic and natural NO_x sources over the U.S. on tropospheric chemistry, *P. Natl. Acad. Sci. USA*, 100, 1505–1509, 2003.